# $^{40}Ar/^{39}Ar$ Geochronology

- History, fundamental issues and assumptions, nomenclature, age equation
- $^{40}Ar/^{39}Ar$ dating in practice
    - gas extraction
    - irradiation, undesirable nuclear reactions and their corrections
    - multi-collector mass spectrometry – ***a revolution***
    - minimizing uncertainties
    - appropriate samples
- Reporting, presentation, and interpretation of complex data sets
    - metadata, age spectrum, isochron, probability/kernal density, rank-order plots
    - evaluation of FCs & ACs standard ages and homogeneity
    - why precision matters and what do dates record?
    - examples: the Bishop Tuff & future challenges
- Calculation of apparent ages and uncertainties
    - standard minerals used to monitor neutron fluence
    - GTS2012 calibrates $^{40}Ar/^{39}Ar$ ages to 28.201 $\pm$ 0.046 Ma Fish Canyon sanidine (FCs) [Kuiper et al., 2008, astronomical basis]
    - Alder Creek sanidine now calibrated to 1.1864 $\pm$ 0.0006 Ma [Jicha et al., 2016]
    - analytical + systematic [decay constant & standard age] uncertainties
- Recalibrating published (legacy) dates [Mercer & Hodges, 2016]

# Roots of $^{40}Ar/^{39}Ar$ geochronology: The K-Ar method

Aldrich & Nier (1948) University of Minnesota

- $^{40}Ar$ is decay product of the rarest naturally occurring isotope of potassium, $^{40}K$
- A potentially useful geochronometer
- $^{38}Ar$ isotope dilution tracer allows measurement of $^{40}Ar^*$ (Wasserburg & Hayden, 1955)

***Potassium*** is 7th most abundant element in crust (2.6 wt.%)

- Common in rock forming minerals
- Isotopic composition of K at any time in geologic history is uniform
  - Presently: $^{41}K$: $^{40}K$: $^{39}K$ = 6.7301: 0.01167: 93.2581
- $^{40}K$ comprises 0.01% of all K. Its radioactive decay is *branched*:
  - 10.48% via electron capture to $^{40}Ar$ ($\lambda_\varepsilon = 0.580 \times 10^{-11}$ yr$^{-1}$)
  - 89.32% via Beta decay to $^{40}Ca$ ($\lambda_\beta = 4.884 \times 10^{-10}$ yr$^{-1}$)
  - **Total decay constant** $\boldsymbol{\lambda_{tot} = 5.463 \pm 0.107 \times 10^{-10}}$ **yr$^{-1}$** [Min 2000/Kuiper, 2008]

***Argon*** is highly variable in isotopic composition owing to radiogenic production from $^{40}K$

- Any closed system will accumulate $^{40}Ar^*$
- Hydrosphere-atmosphere contains following proportions (Nier, 1950, Phys. Rev.)
- $^{40}Ar$: $^{38}Ar$: $^{36}Ar$ = 99.60 : 0.0632 : 0.3364 [$^{40}Ar/^{36}Ar_{air} = 295.5 \pm 0.5$]
- Recent revision of $^{40}Ar/^{36}Ar$ in air to 298.56 ± 0.31 (Lee et al., 2006)
- Argon is an inert gas—*not bound to any mineral lattice*
  - Thus loss of $^{40}Ar^*$ via diffusion is common

WiscAr

## The K-Ar age equation

$$t = \frac{1}{\lambda} \ln\left[1 + \frac{D}{P}\right]$$

$P$ = number of radioactive atoms at time $t$,
$D$ = number of daughter atoms at $t$.

$$t = \frac{1}{\lambda} ln\left[1 + \left(\frac{\lambda}{\lambda_e}\right)\left(\frac{{}^{40}Ar^*}{{}^{40}K}\right)\right]$$

Recall branched decay of $^{40}K$ to $^{40}Ar$ such that $\lambda/\lambda_\varepsilon = 9.54$

Must determine concentrations of $^{40}K$ and $^{40}Ar^*$ in mol/g independently

- Determine K by flame photometry (on separate split of solid mineral or rock)
- Determine $^{40}Ar^*$ by isotope dilution mass spectrometry
  - Add calibrated volume of $^{38}Ar$ tracer as an isotope dilution spike.
  - Abundance of $^{40}Ar$ determined by relative abundances of $^{40}Ar$ to $^{38}Ar$ in sample
  - Also possible to determine $^{40}Ar$ manometrically by adjusting volume/pressure in mass spectrometer—the "unspiked" K-Ar technique.
- Correction for $^{40}Ar_i$ (this is the $^{40}Ar$ present at the time the mineral or rock forms)
  - $^{40}Ar^*$ - $^{40}Ar_t$ - $^{40}Ar_i$
  - Assume all $^{40}Ar_i$ derives from atmosphere in which: $^{40}Ar = 298.56 \times {}^{36}Ar$
  - Thus, $^{40}Ar^* = {}^{40}Ar_t - (298.56 \times {}^{36}Ar)$

Journal of Geophysical Research Vol. 71, No. 11 June 1, 1966

# Potassium-Argon Dating by Activation with Fast Neutrons

Craig Merrihue[1] and Grenville Turner[2]

*Department of Physics, University of California, Berkeley*

When a potassium-bearing mineral is irradiated by a neutron flux containing a significant fraction of fast neutrons, 270-year $Ar^{39}$ is produced by the $K^{39}$ $(n, p)$ reaction, and this may be used as a basis for measuring the potassium-argon age of the mineral. *Wänke and Konig* [1959] described such a method in which counting techniques were used to detect the $Ar^{39}$, as well as $Ar^{41}$ produced by the $Ar^{40}$ $(n, \gamma)$ reaction. A calculation of the potassium content for a single sample would require a knowledge of the flux-energy distribution in the reactor and the excitation function of the $K^{39}$ $(n, p)$ reaction. The uncertainties of this calculation can be avoided, however, by comparing the $(Ar^{40}/Ar^{39})$ ratio in the unknown sample with that quantity in a sample of known age, given the same irradiation. In this case we may write down the following relationships.

$$\frac{(Ar^{40}/K^{40})}{(Ar^{40}/K^{40})_s} = \frac{(Ar^{40}/Ar^{39})}{(Ar^{40}/Ar^{39})_s} = \frac{(Ar^{41}/Ar^{39})}{(Ar^{41}/Ar^{39})_s}$$

$$= \frac{(\exp(T/\tau) - 1)}{(\exp(T_s/\tau) - 1)} \quad (1)$$

$T$ is the unknown potassium-argon age, $\tau$ is the mean life of $K^{40}$, and the subscript $s$ refers to the sample of known age.

A correction for atmospheric contamination is not possible with this technique, and more recently *Merrihue* [1965] has suggested using mass spectrometric detection of the $Ar^{39}$ and radiogenic $Ar^{40}$. The method has the advantage of allowing $Ar^{36}$ to be measured, and, conse-

[1] Dr. Craig Merrihue was killed in a climbing accident on Mount Washington, New Hampshire, on March 14, 1965.

[2] Present address: Department of Physics, Sheffield University, England.

# The $^{40}Ar/^{39}Ar$ age equation

in fast neutron flux:

$$^{39}Ar_K = {}^{39}K \Delta \int \phi(E)\sigma(E)dE$$

$^{39}Ar_K$ : no. of atoms of $^{39}Ar$ produced from $^{39}K$
$^{39}K$ : original number of $^{39}K$ atoms present
$\Delta$ : duration of irradiation
$\Phi(E)$ : neutron flux at energy $E$
$\sigma(E)$ : neutron capture cross section at energy $E$ for $^{39}K(n,p)^{39}Ar$ nuclear reaction

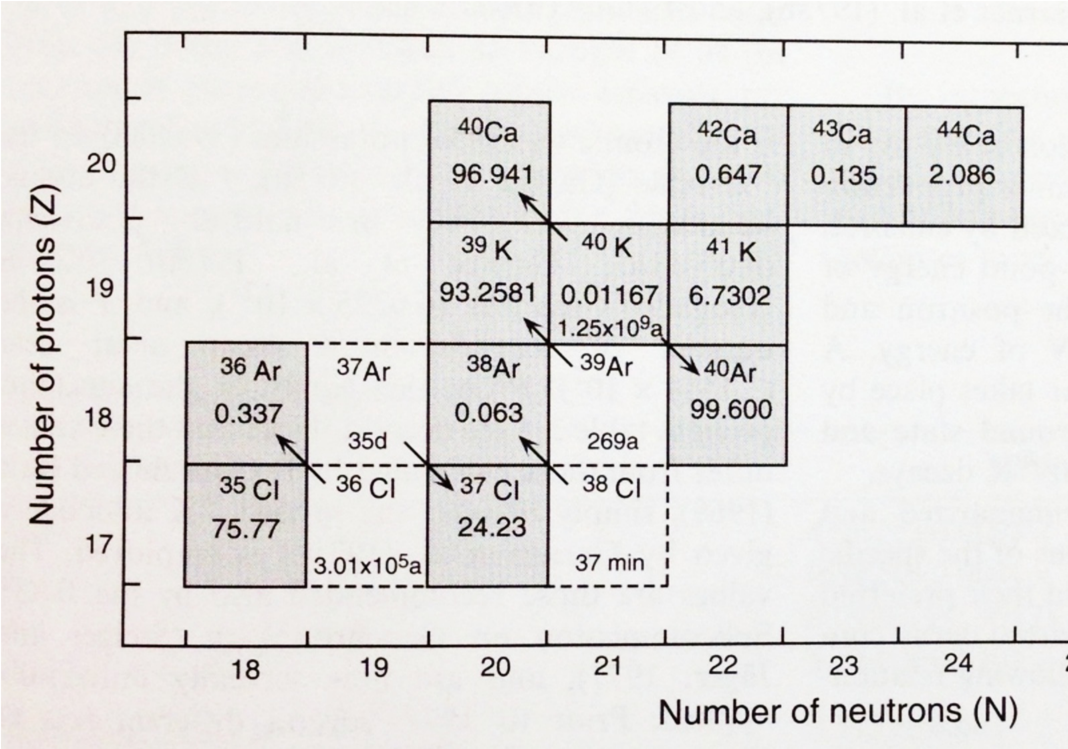


McDougall and Harrison (1999)

$$\frac{^{40}Ar^*}{^{39}Ar_K} = \frac{^{40}K}{^{39}K}\frac{\lambda_{ec}}{\lambda}\frac{1}{\Delta}\frac{[e^{\lambda t}-1]}{\int \phi(E)\sigma(E)dE}$$

define dimensionless parameter, J:

$$J = \frac{^{39}K}{^{40}K}\frac{\lambda}{\lambda_{ec}}\Delta \int \phi(E)\sigma(E)dE$$

$J$ is a measure of the proportion of $^{39}K$ converted to $^{39}Ar$ and thus total K in sample assuming the $^{39}K/K_{total}$ ratio is constant in nature

# The $^{40}Ar/^{39}Ar$ age equation

$J$ is determined by measuring $^{40}Ar^*/^{39}Ar_K$ in standard of known $t$

The $J$ value is determined by measuring the $^{40}Ar^*/^{39}Ar_K$ ratio in several crystals of a neutron fluence monitor that is co-irradiated (adjacent to) with the unknown samples


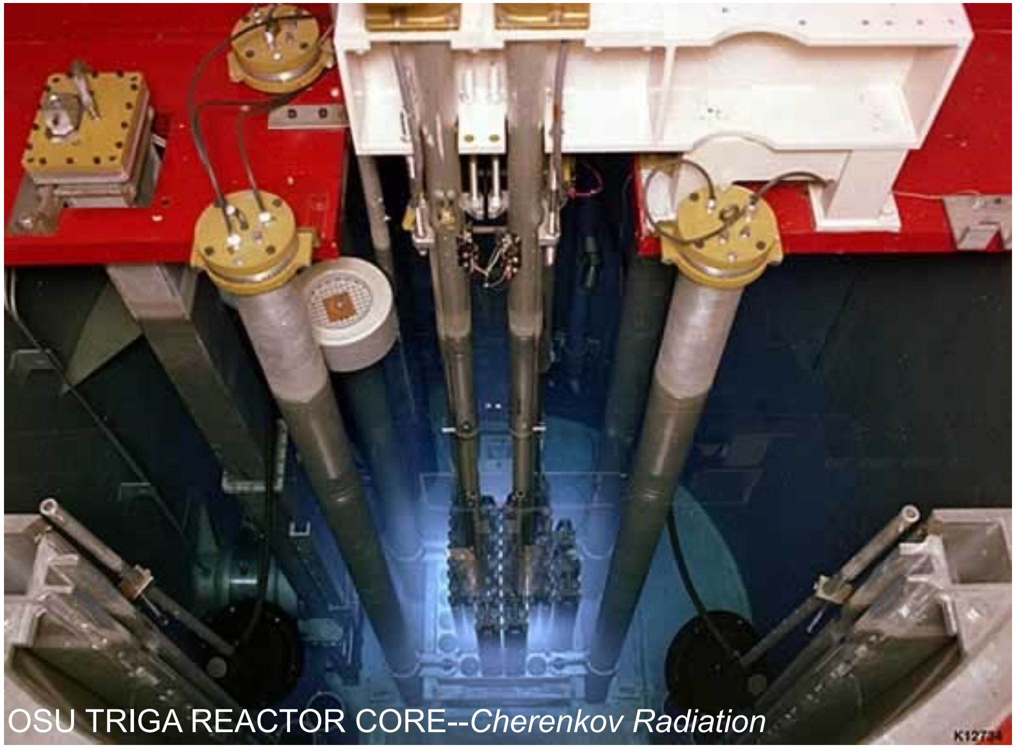


OSU TRIGA REACTOR CORE--*Cherenkov Radiation*

The most widely used mineral standard is sanidine from the **Fish Canyon tuff (FCs)** with an age of **28.201 ± 0.046 Ma**, determined through astrochronologic calibration by Kuiper et al (2008)

*In practice:*

$$t = \frac{1}{\lambda}\ln\left[1 + J\,\boxed{\frac{^{40}Ar^*}{^{39}Ar_K}}\right]$$

1. measure $^{40}Ar/^{39}Ar$ ratio in sample; insert J value from step 2; calculate $t$

$$J = \frac{e^{\lambda t} - 1}{\left[\boxed{{}^{40}Ar^* / {}^{39}Ar_K}\right]}$$

2. measure $^{40}Ar/^{39}Ar$ ratio in standard mineral

# Argon nomenclature

- ***Atmospheric argon***: Argon with isotopic composition found in present day atmosphere ($^{40}Ar/^{36}Ar = 298.56$).

- ***Radiogenic argon:*** Argon formed from *in-situ* decay of $^{40}K$ in a rock or mineral (commonly denoted- $\mathbf{^{40}Ar^{*}}$)

- ***Trapped argon***: Argon incorporated into rock of mineral at time of its formation or during a subsequent event. For terrestrial samples this is commonly but not always the atmospheric composition. *(equivalent to the initial $^{87}Sr/^{86}Sr$ ratio in Rb-Sr isotope studies).*

- ***Cosmogenic argon:*** Argon produced from cosmogenic ray interactions with target nuclei Ca, Ti, Fe (spallation and neutron capture reactions).

- ***Neutron-induced argon:*** Argon produced in sample during irradiation in nuclear reactor, owing to neutron interactions with Cl, K, and Ca.

- ***Extraneous argon***: If trapped argon in terrestrial samples has $^{40}Ar/^{36}Ar > 298.6$, the additional $^{40}Ar$ is referred to as ***extraneous*** argon:
  - **Excess argon**: that component of $^{40}Ar$, apart from atmospheric argon, incorporated into samples by processes other than *in situ* radioactive decay of $^{40}K$ (fluid infiltration, unequilibrated mantle contribution carried in magma).
  - **Inherited argon**: that $^{40}Ar$, essentially radiogenic, introduced into a rock or mineral sample by physical contamination from older material (beware xenocrysts!).

WiscAr

# Basic assumptions

## *Decay Constant*

- Parent nuclide $^{40}K$ decays at rate independent of physical state, P, T, or X
- $\lambda = 5.463 \times 10^{-10}\ y^{-1}$; half-life $t_{½} = 1.25 \times 10^{9}$ y [Min et al., 2000].

## *Constant $^{40}K/K_{tot}$*

- Ratio in nature is constant in all materials today (required because $^{40}K$ not measured directly). We measure $K_{tot}$ (K-Ar) or $^{39}Ar_K$ ($^{40}Ar/^{39}Ar$); $^{40}K$ is derived from the isotopic composition of K
- The ratio has changed over time due to radioactive decay, but this term does not enter into the age equation. At any given time, the ratio was constant in all materials, because isotopes are not fractionated from one another by geological processes.

## *Initial $^{40}Ar$ can be quantified*

- $^{40}Ar^*$ measured was produced by in situ decay of $^{40}K$ in the interval since the rock crystallized or was recrystallized. Violations of this assumption are common: beware excess or inherited argon
- Corrections can be made for non radiogenic $^{40}Ar$ present in the rock being dated. Assume all such argon is atmospheric with $^{40}Ar/^{36}Ar = 298.6$ for initial (model) purposes, Isotope correlation diagrams (isochron regression) may test this.

## *Closed System*

- The sample must have remained a closed to the loss or gain of K or $^{40}Ar^*$ other than by radioactive decay. Departures from this are common in complex, thermally effected, or altered rocks

- ***These assumptions must be assessed in each study undertaken***
- ***An important advantage of $^{40}Ar/^{39}Ar$ method is that basic assumptions underlying calculation and interpretation of age are more readily assessed than is the case for K-Ar age measurements***

# What are we dating?

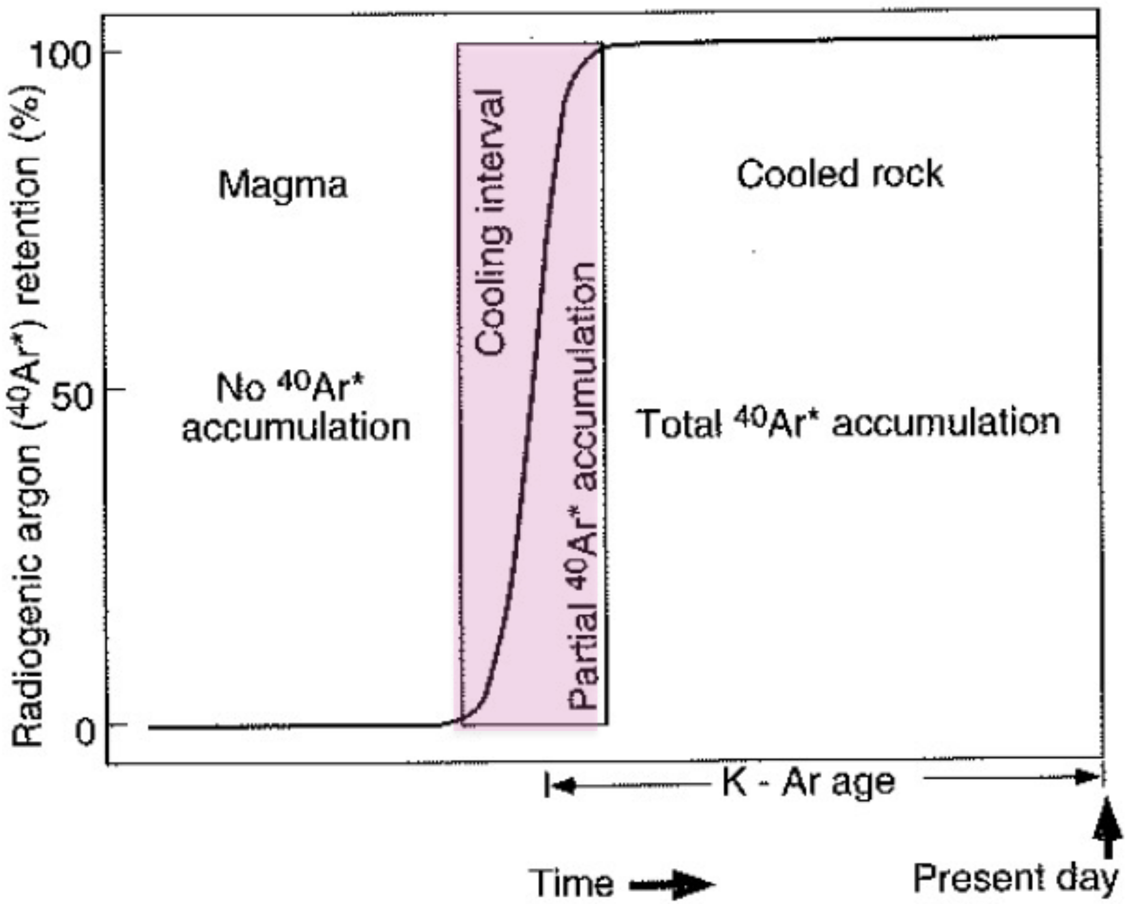


Dalrymple and Lanphere (1969)
McDougall and Harrison (1999)

# Undesirable nuclear reactions

A principal difficulty with $^{40}Ar/^{39}Ar$ method is the production of isotopes of argon from neutron interactions with isotopes of Ca, K, Ar, Cl

- The following interfering reactions are important:
  - $^{40}Ca(n, n\alpha)$**$^{36}Ar$** *(interferes w/atmospheric correction)*
  - $^{42}Ca(n, \alpha)$**$^{39}Ar$**
  - $^{40}K(n, p)$**$^{40}Ar$**
- **Fortunately an isotope of $^{37}Ar$ that does not occur in nature is also produced**
  - $^{40}Ca(n, \alpha)$**$^{37}Ar$**



Box 2. $^{40}Ar/^{39}$ Isotopic Dating Scheme

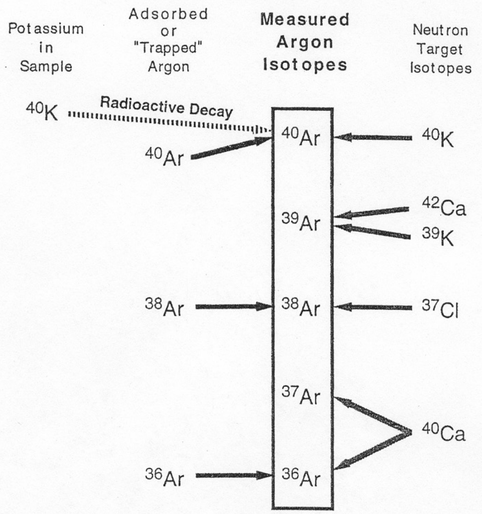


This diagram shows principal sources of the five argon isotopes measured for $^{40}Ar/^{39}Ar$ dating under typical terrestrial conditions: 1) in situ radioactive decay of potassium; 2) entrapment of magmatic argon at the time of crystallization, or subsequently adsorbed onto crystal surfaces or incorporated within the grain due to alteration; or 3) neutron-induced reactions on target elements during irradiation. To summarize the $^{40}Ar/^{39}Ar$ isotopic dating scheme, $^{40}Ar$ is principally derived from radiogenic decay of $^{40}K$ or from contamination by atmospheric argon; the extent of contamination is determined by the abundance of $^{36}Ar$ (the $^{40}Ar/^{36}Ar$ ratio of air is 295.5[1]). $^{39}Ar$ is derived by neutron-induced reactions on $^{39}K$ in the nuclear reactor. Neutron reactions on Ca during irradiation also produce the interfering isotopes $^{36}Ar$ and $^{39}Ar$, which can be minimized by shortening the time the samples are kept in the reactor. $^{37}Ar$, which is derived principally from Ca during irradiation, is used as the isotopic reference to correct for these interferences. The relative proportions of argon isotopes produced from reactions on Ca are calibrated by irradiation and measurement of "pure" $CaF_2$ (optical grade fluoride). One further interference of signifi-cance is the production of $^{40}Ar$ from $^{40}K$ during irradiation; the extent of this reaction can be greatly minimized by using cadmium shielding of the sample package in the reactor. In addition,this interference can be corrected for by measurement of the $^{40}Ar/^{39}Ar$ production ratio of the reactor through the use of an artificial K-bearing, $^{40}Ar^*$- and Ca-free material.

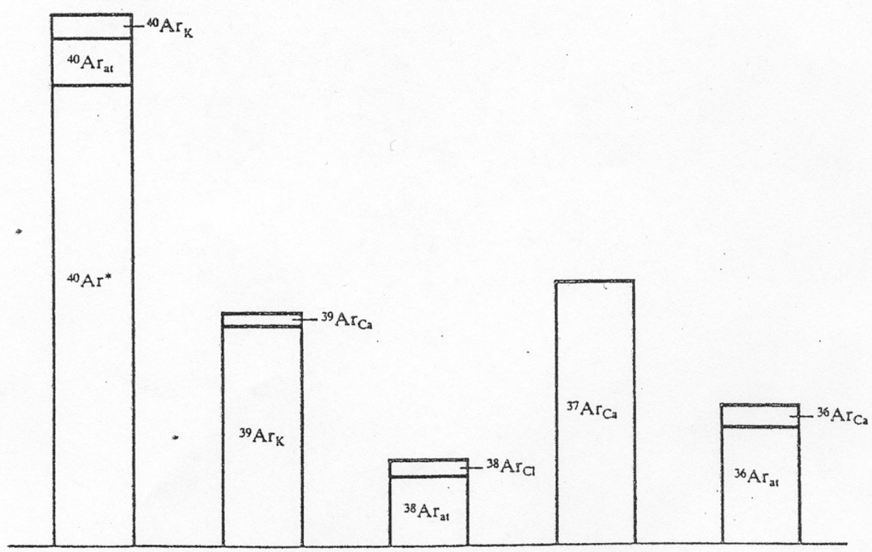


*Figure 1.* Mass spectrum of an irradiated mineral (between mass 40 and mass 36), wit emphasis on the origin of different components. Subscripts refer to the original elemen Relative amounts are not respected.

*Deino*

*Dalrymple & Lanphere (1969)*

WiscAr

# Undesirable nuclear reactions

**$^{37}Ar$ is produced by the $^{40}Ca(n,\alpha)^{37}Ar$ reaction**

- $^{37}Ar$ is *radioactive* with $t_{½}$ = 35.1 days
- must calculate initial $^{37}Ar$ following irradiation: $^{37}Ar_o = {}^{37}Ar_m e^{\lambda_{37}t}\lambda_{37}t_i / (1-e^{-\lambda_{37}t_i})$
  - *t = irradiation time*
  - *$t_i$ = time between irradiation and analysis*
  - *$\lambda_{37}$ = decay constant of $^{37}Ar$ = 0.01974/day*

- permits corrections for undesirable Ca- and K-derived Ar

- corrections require measurement of 3 reactor constants:
  - $[^{40}Ar/^{39}Ar]_K$
  - $[^{36}Ar/^{37}Ar]_{Ca}$
  - $[^{39}Ar/^{37}Ar]_{Ca}$

- Corrections are based on replicate analyses of K-free Ca salt ($CaF_2$) and Ca-free salt (K-Fe-$SiO_2$) using ratios with $^{37}Ar$, $^{38}Ar$, $^{40}K$

# Undesirable nuclear reactions

Production of $^{40}Ar$ from $^{40}K$ is variable by order of magnitude from reactor to reactor. This must be corrected carefully in each irradiation, ideally with long-term characterization

*In pure kalsilite (K-Fe-$SiO_2$), Ca-free glass* $^{39}Ar_K = {}^{39}Ar_m$ (m = measured value)

$$[^{40}Ar/^{39}Ar]_K = (^{40}Ar_m - {}^{36}Ar_m * 298.6)/^{39}Ar_m$$

*In pure CaF salt, $^{36}Ar$ is from $^{40}Ca$ and air, and $^{39}Ar$ is from $^{42}Ca$, so:*

$$[^{36}Ar/^{37}Ar]_{Ca} = (^{36}Ar_m - {}^{40}Ar_{air}/298.6)/^{37}Ar_m$$

$$[^{39}Ar/^{37}Ar]_{Ca} = (^{39}Ar_m / {}^{37}Ar_m)$$

Correction factors for **cadmium-shielded** irradiations in the CLICIT (cadmium-lined in-core irradiation tube) at the Oregon State University based on UW-Madison and Berkeley Geochronology Center data:

$$[^{40}Ar/^{39}Ar]_K = 0.00054 \pm 0.00014$$

$$[^{36}Ar/^{37}Ar]_{Ca} = 0.000265 \pm 0.000002$$

$$[^{39}Ar/^{37}Ar]_{Ca} = 0.000695 \pm 0.000009$$

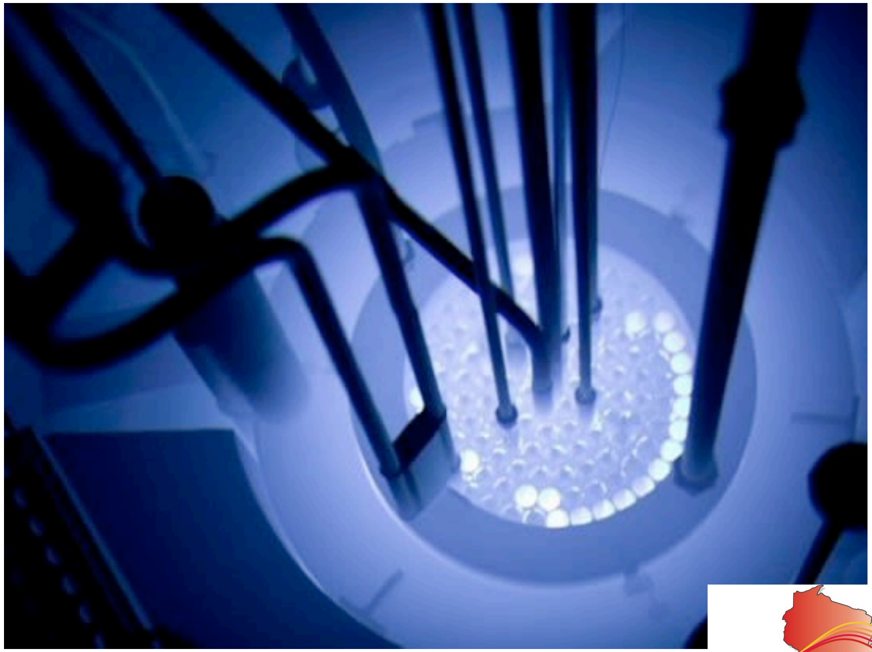

WiscAr

# Calculation of apparent ages and analytical uncertainties

## *Calculation of $^{40}Ar^*/^{39}Ar$*

m = measured

Ca = neutron induced on Ca

K = neutron induced on K

A = atmospheric ($^{40}Ar/^{36}Ar = 298.6$)

$$\left[\frac{^{36}Ar}{^{37}Ar}\right] = \left[\frac{^{36}Ar_m - {}^{40}Ar_A/298.6}{^{37}Ar}\right]$$

$^{40}Ar_m = {}^{40}Ar^* + {}^{40}Ar_A + {}^{40}Ar_K + {}^{40}Ar_{Ca}$ (3.34)

$^{40}Ar^* = {}^{40}Ar_m - {}^{40}Ar_A - {}^{40}Ar_K$ *($^{40}Ar_{Ca}$ very small; effectively taken into account by atmospheric correction)* (3.35)

$^{36}Ar_m = {}^{36}Ar_A + {}^{36}Ar_{Ca}$ (3.36)

$^{40}Ar_A = 298.6*[{}^{36}Ar_m - {}^{36}Ar_{Ca}]$ (3.37)

substitute 3.37 into 3.35:

$^{40}Ar^* = {}^{40}Ar_m - 298.6*{}^{36}Ar_m + 298.6*{}^{36}Ar_{Ca} - {}^{40}Ar_K$ (3.38)

$^{39}Ar_m = {}^{39}Ar_K + {}^{39}Ar_{Ca}$ , so that (3.39)

$^{39}Ar_K = {}^{39}Ar_m - {}^{39}Ar_{Ca}$ (3.40)

Divide 3.38 by 3.40 and both numerator and denominator by $^{39}Ar_m$

$$\frac{^{40}Ar^*}{^{39}Ar_K} = \left[\frac{(^{40}Ar/^{39}Ar)_m - 298.6(^{36}Ar/^{39}Ar)_m + 298.6(^{36}Ar/^{37}Ar)_{Ca}(^{40}Ar_K/^{39}Ar)_m}{1-(^{39}Ar_{Ca}/^{37}Ar_m)}\right] \quad (3.41)$$

*McDougall and Harrison (1999)*

## Calculation of apparent ages and analytical uncertainties

As:

$$\frac{^{36}Ar_{Ca}}{^{39}Ar_m} = \frac{^{36}Ar_{Ca}}{^{37}Ar_{Ca}} \frac{^{37}Ar_m}{^{39}Ar_m} = \left[\frac{^{36}Ar}{^{37}Ar}\right]_{Ca} \left[\frac{^{37}Ar}{^{39}Ar}\right]_m$$

because $^{37}Ar_{Ca} = {}^{37}Ar_m$, and

$$\frac{^{39}Ar_{Ca}}{^{39}Ar_m} = \frac{^{39}Ar_{Ca}}{^{37}Ar_{Ca}} \frac{^{37}Ar}{^{39}Ar_m}$$

for the same reason:

$$\frac{^{40}Ar_K}{^{39}Ar_m} = \left[\frac{^{40}Ar}{^{39}Ar}\right]_K \frac{^{39}Ar_K}{^{39}Ar_m} = \left[\frac{^{40}Ar}{^{39}Ar}\right]_K \left[1 - \frac{^{39}Ar_{Ca}}{^{39}Ar_m}\right]$$

we can re-write 3.41:

$$\frac{^{40}Ar^*}{^{39}Ar_K} = \left[\frac{(^{40}Ar/^{39}Ar)_m - 298.6(^{36}Ar/^{39}Ar)_m + 298.6(^{36}Ar/^{37}Ar)_{Ca}(^{37}Ar/^{39}Ar)_m}{1-(^{39}Ar/^{37}Ar)_{Ca}(^{37}Ar/^{39}Ar)_{Ca}}\right] - \left[\frac{^{40}Ar}{^{39}Ar}\right]_K$$

*McDougall and Harrison (1999)*

# Calculation of apparent ages and analytical uncertainties

1. errors for each ratio in 3.42 are obtained from the least squares regression of peak height to time of inlet of gas to spectrometer.
2. these can be combined quadratically with other errors (e.g., mass discrimination) to give overall error estimate for given ratio.
3. error in $^{40}Ar^*/^{39}Ar_K$ is complex function of all errors in eq. 3.42.
   a. error magnification as proportion of $^{40}Ar_A$ increases as well.
4. Dalrymple and Lanphere (1971) derived error formula by differentiation of 3.42. The variance (st. dev. squared) of the $^{40}Ar^*/^{39}Ar_K$ ratio is given by:

$$F^2_F = F^2_G + C^2_1F^2_B + [C_4G - C_1C_4B + C_1C_2]^2F^2 \qquad (3.43)$$

$F = {}^{40}Ar^*/^{39}Ar_K$

$G = (^{40}Ar/^{39}Ar)_m$

$B = (^{36}Ar/^{39}Ar)_m$

$D = (^{37}Ar/^{39}Ar)_m$

$C_1 = (^{40}Ar/^{36}Ar)_A = 298.6$

$C_2 = (^{36}Ar/^{37}Ar)_{Ca}$

$C_3 = (^{40}Ar/^{39}Ar)_K$

$C_4 = (^{39}Ar/^{37}Ar)_{Ca}$

This gives errors for individual gas analysis. However, age equation also includes *J*:

$$t = \frac{1}{\lambda}\ln\left[1 + J\frac{^{40}Ar^*}{^{39}Ar_K}\right]$$

For error in age calculated from the $^{40}Ar^*/^{39}Ar_K$ ratio, we must also include error in *J*:

$$F^2_t = [J^2F^2_F + F^2F_J^2] / [\lambda^2(1+FJ)^2] \qquad (3.44)$$

***Typical errors in J are of the order <0.2 % of the measured value***

For all sub-samples from which measured $^{40}Ar/^{39}Ar$ are converted to t using a single *J* value, this error in *J* i calculated.

*McDougall and Harrison (1999)*

WiscAr

# $^{40}Ar/^{39}Ar$ dating in practice gas extraction, clean up, mass spectrometry

**Automated gas handling**

- heating
- gas clean-up
- inlet to mass spectrometer
- 15 – 45 min analysis time

**Mass spectrometers**

- Single collector, Secondary Electron Multiplier (SEM) detector, peak scanning
- Multi-collector instruments, 5 detectors, including either ion counting multipliers, Faraday collectors, or both

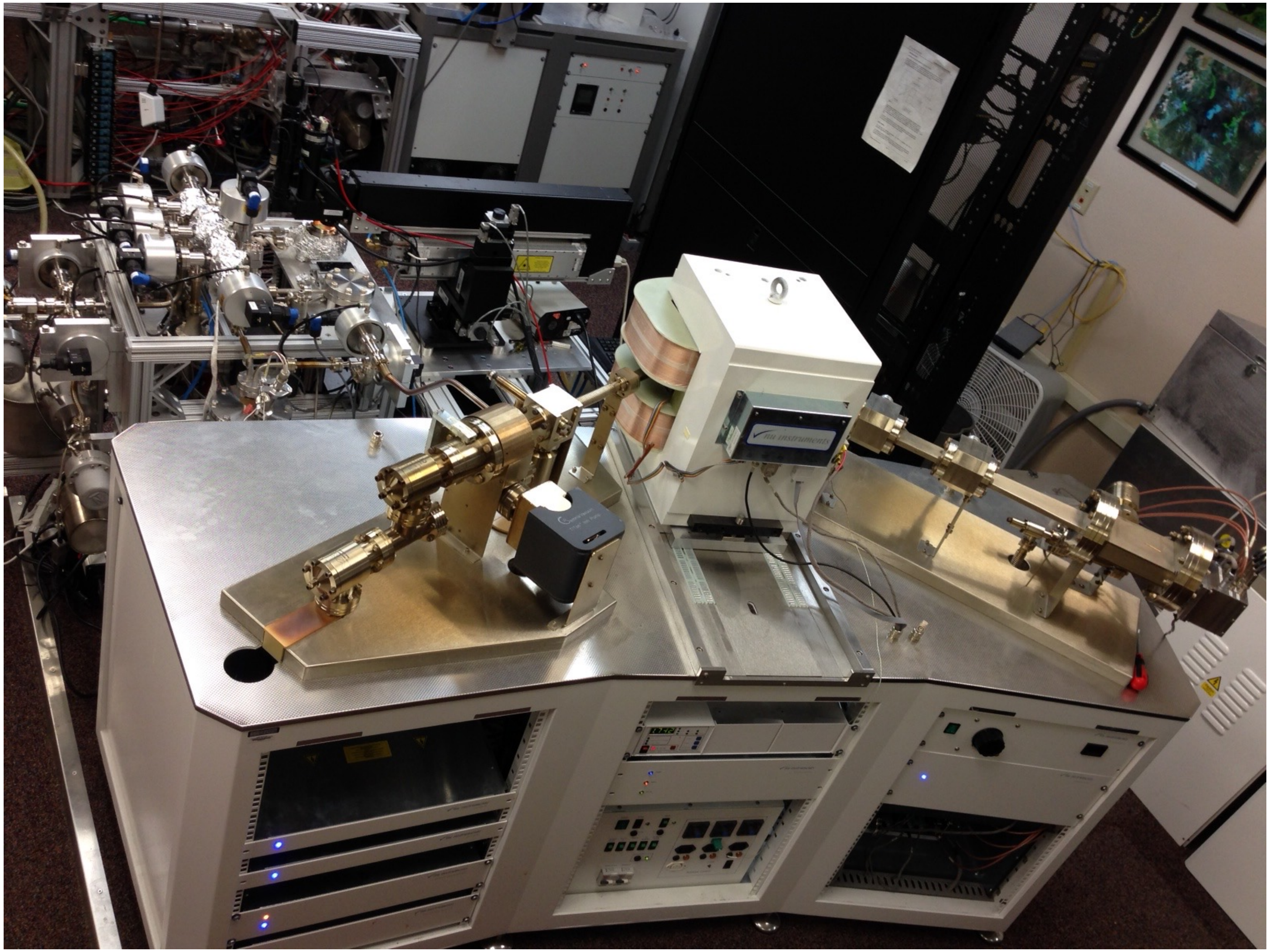

# Materials useful for $^{40}Ar/^{39}Ar$ dating

## Volcanic rocks (useful for time scale and stratigraphic studies)

- Minerals
  - **Sanidine (to 2 ka)**
  - **Anorthoclase (to 5 ka)**
  - Plagioclase (to 200 ka)
  - Amphibole (to 1 Ma)
  - Biotite
  - Leucite
  - Nepheline
- Whole-rock material
  - **Groundmass concentrate (to 3-4 ka)**
  - Non-hydrated glass (to 300 ka)

## Plutonic, metamorphic, ore minerals

- K-spar
- Plagioclase
- Biotite
- Amphibole
- Muscovite
- Phengite
- Alunite
- Adularia

## Sediments

- Clays (encapsulated fusion)
- Glauconite (“)
- Evaporites (e.g., langbeinite, $K_2Mg_2(SO_4)_3$ )
- Detrital K-bearing minerals
- Alunite/jarosite as weathering products

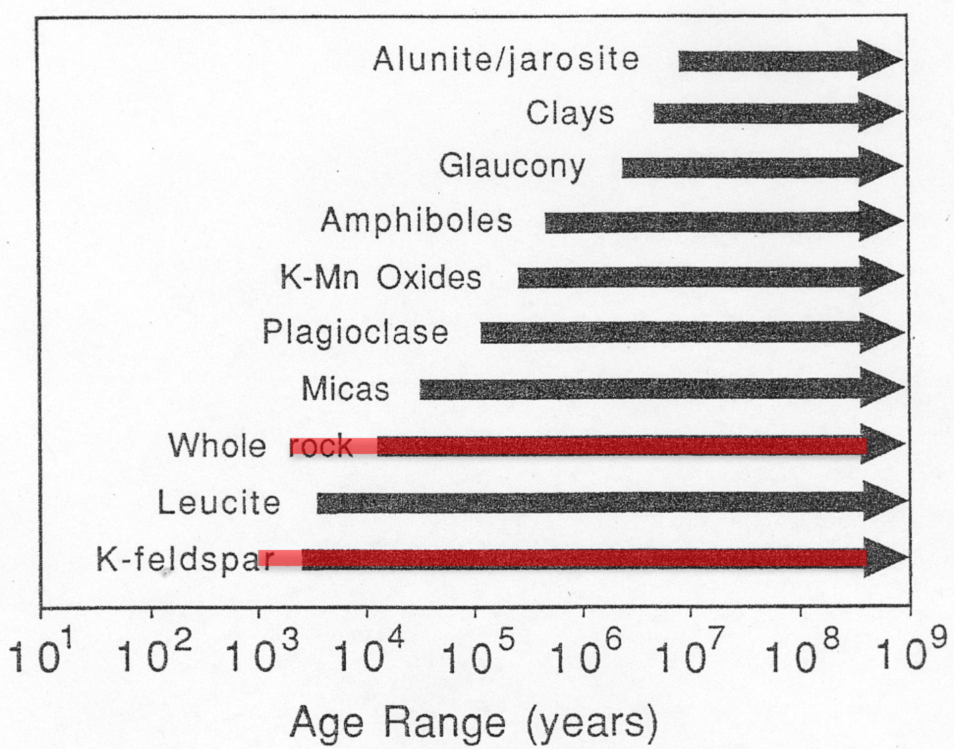


Figure 4. Age range of K-Ar and $^{40}Ar/^{39}Ar$ dating applicability for various materials.

*Renne, 2000*

# Sampling - Lavas

- "The first step of any geochronological analysis involves selecting the sample". *Reiners et al. Geochronology and Thermochronology (2017)*

- Target the slowly cooled interior of the lava flow
  - *Avoid outer skin or rubbly base*
  - *Avoid oxidized/vesicular sections*
  - *Avoid sampling close to intrusions*
  - *Take good notes!!*

# Sampling - Tephra

- Tephra is commonly crystal-poor and fine-grained
  - *Sample from crystal-rich portions of the deposit*
  - *Collect sufficient material for multiple chronometers & methods*
  - *Avoid contamination from surrounding beds*


# Sample preparation – Tephra & Bentonite

Crushing and sieving
↓
Gold table
↓
Magnetic separation
↓
Acid leaching (as needed)
↓
Heavy Liquids separation
↓
Hand picking
↓
SEM verification

- Optical microscopy
- SEM to verify purity of mineral separation
- Iterate heavy liquids separations if needed

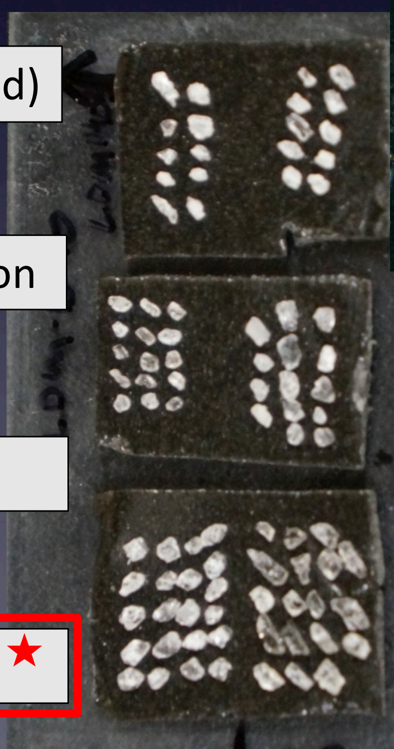

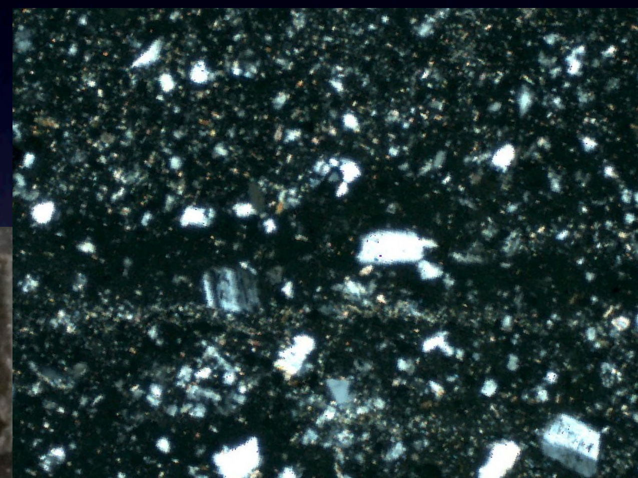

150 micron feldspars in Eocene Main tuff Wilkins Peak Member, Green River Fm

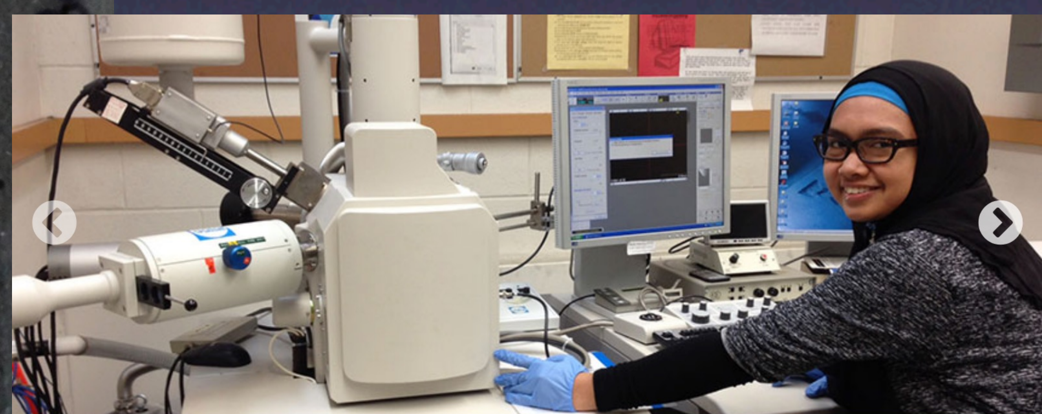

**The Cameron Electron Microscope Laboratory**. This Scanning Electron Microscope is used to screen crystals of feldspar prior to irradiation.

# A note on sample sizes for multi-collector mass spectrometry

- How much material do I need to analyze?

modified from McDougall & Harrison (1999)

- Need ≈ $10^{-14}$ to $10^{-15}$ moles of radiogenic $^{40}Ar$ per analysis

- ***Sanidine*** crystals contain 10-14% $K_2O$
- ***Basalt*** 1-2% $K_2O$
- ***Rhyolite*** 3-5% $K_2O$

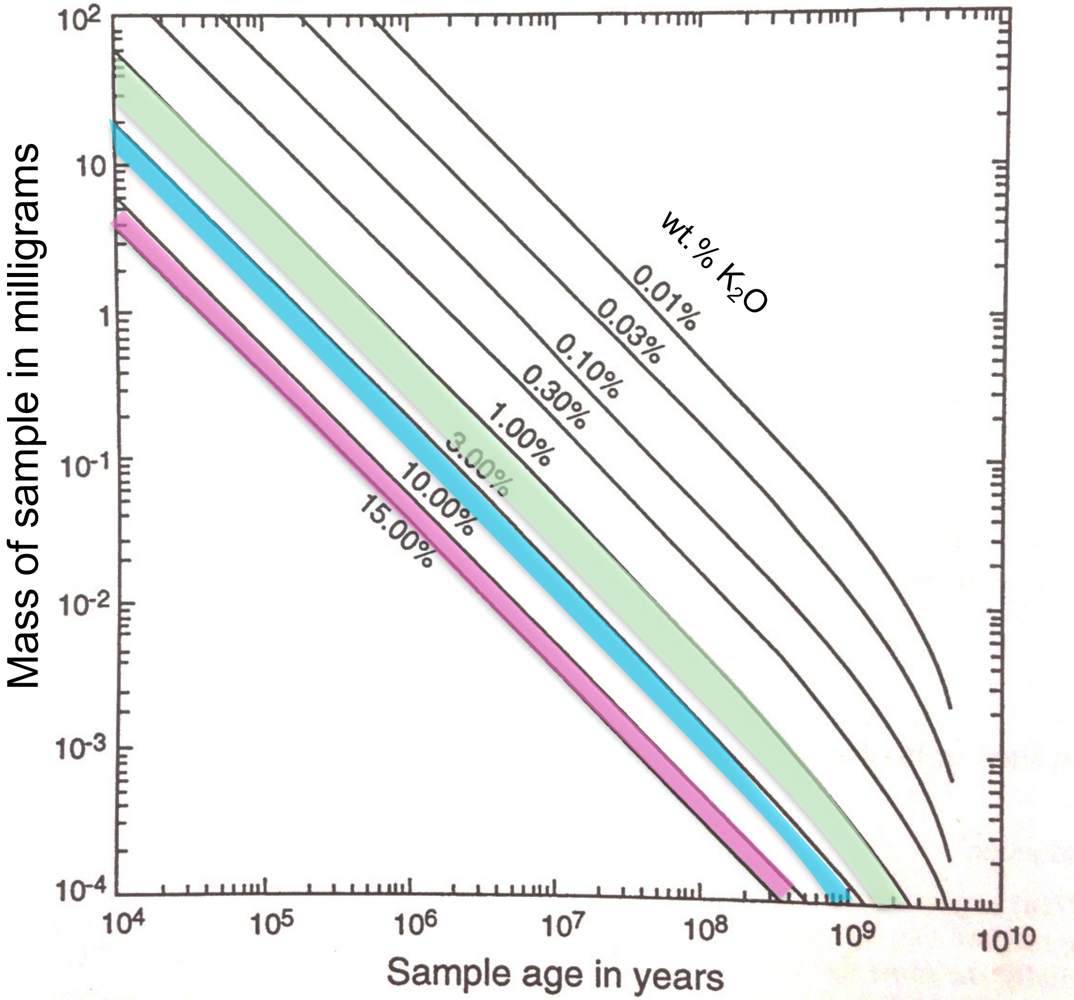


*Mass of sample required to yield **1 x $10^{-15}$** moles of radiogenic argon for a given age. Potassium content (wt.%) is indicated on the curves.*

Rules of thumb:

- ***A millimeter diameter sanidine phenocryst = 2 mg***
- *Silt sized sanidines = 0.1 mg*
- *For an incremental heating analysis, need 10X more sample*

WiscAr

# Analysis - Gas extraction

- Infrared laser heating
  - 10.6 μm wavelength $CO_2$ laser
  - Incremental-heating or total fusion of small samples/single crystals

10 mg basalt groundmass

60 mm

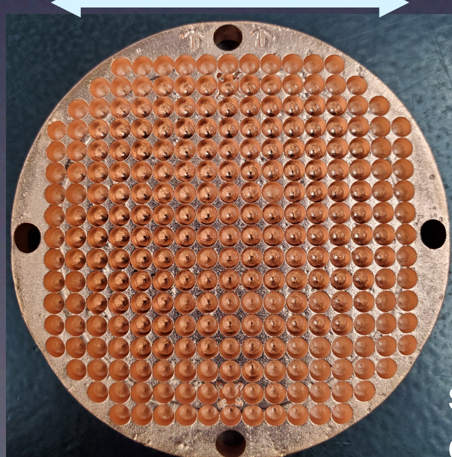

1 mg sanidine crystals

- Ultraviolet laser ablation
  - 193 nm excimer laser
  - *In-situ* analyses
  - 2-150 micron resolution

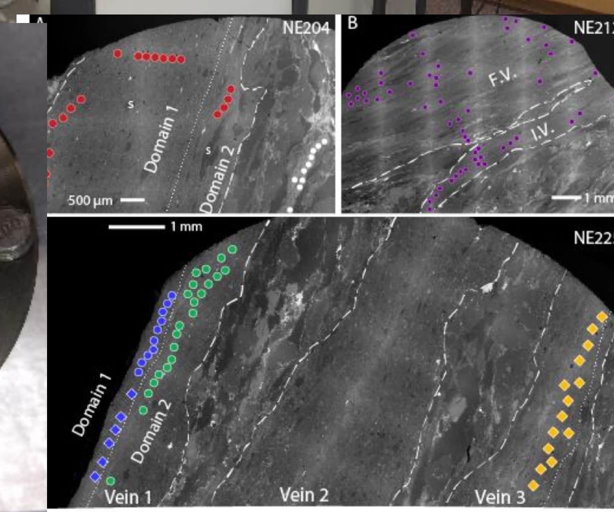

# Estimated analytical uncertainties

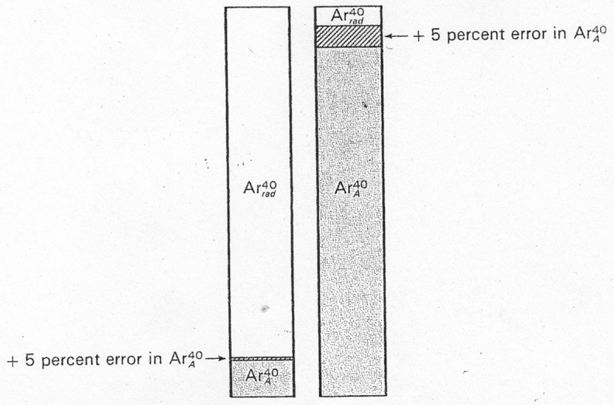


FIGURE 7-3
An error in the atmospheric argon correction is much more serious when the radiogenic argon percentage is small than when it is large.

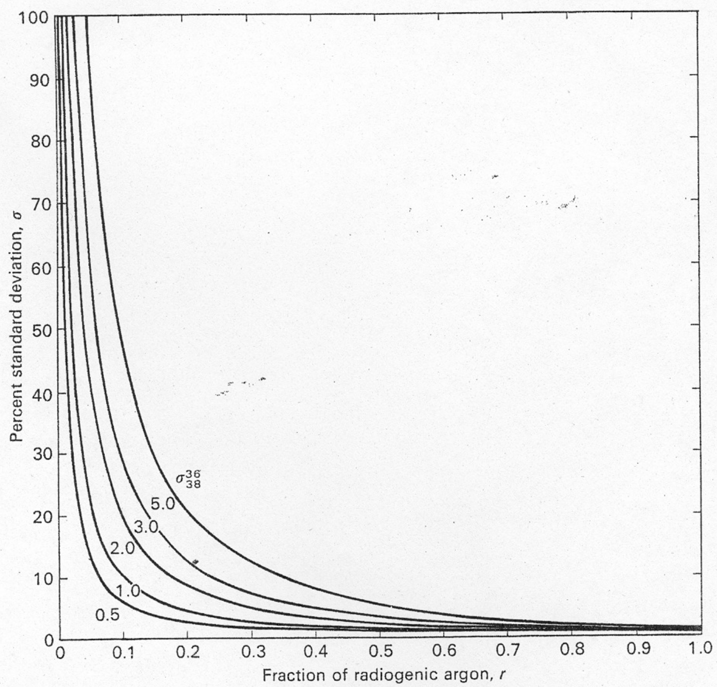


FIGURE 7-4
Percentage standard deviation, $\sigma$, in a potassium-argon age as a function of the fraction of radiogenic argon, $r$, for various values of $\sigma^{36}_{38}$. The curves were calculated from equation (7-1) using $\sigma_k = 0.5$ percent, $\sigma_z = 0.3$ percent, and $\sigma^{40}_{38} = 0.2$ percent. [After A. Cox and G. B. Dalrymple, Jour. Geophys. Res., v. 72, p. 2603-2614, 1967.]

*Dalrymple and Lanphere, 1969*

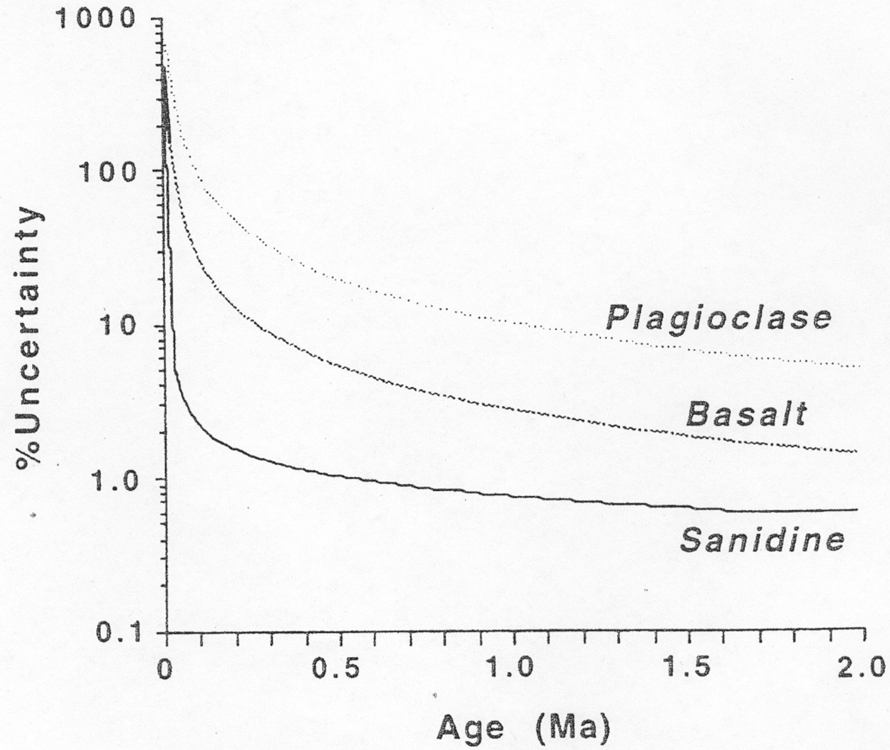


Figure 7. Results of error modeling for three compositionally distinct samples; based on parameters discussed in text. Plagioclase has 0.25 percent K, Ca/K = 10; Basalt has 1.0 percent K, Ca/K = 10; Sanidine has 10 percent K, Ca/K = 0.005.

*Renne, 2000*

WiscAr

## Data reporting in $^{40}Ar/^{39}Ar$ geochronology

**Table 1**
Ar/Ar data and constants used in age calculations. All errors shown at $1\sigma$. Columns in grey are optional but recommended.

Sample: SH-10 — Lab #: 33018-23 — $J$: 0.026703 ± 0.000035 — $D^1$: 1.0066 ± 0.0028 — Heating: 60 s

Plagioclase — IGSN #: PRR001S35

Irradiation coordinates: $x = 0.53$ cm; $y = 0.85$ cm; $z = 0.31$ cm

| N | Power (W) | $^{40}$Ar (moles) | $^{40}$Ar ($10^{-9}$ A) | $\pm\sigma_{40}$ ($10^{-12}$ A) | $^{39}$Ar ($10^{-10}$ A) | $\pm\sigma_{39}$ ($10^{-13}$ A) | $^{38}$Ar ($10^{-12}$ A) | $\pm\sigma_{38}$ ($10^{-14}$ A) | $^{37}$Ar ($10^{-9}$ A) | $\pm\sigma_{37}$ ($10^{-12}$ A) | $^{36}$Ar ($10^{-13}$ A) | $\pm\sigma_{36}$ ($10^{-14}$ A) | %$^{40}$Ar* | $^{40}$Ar*/$^{39}$Ar$_K$ |
|---|---|---|---|---|---|---|---|---|---|---|---|---|---|---|
| A | 0.5 | 1.02E−15 | 0.09713 | 0.43 | 0.13065 | 0.75 | 0.1826 | 1.40 | 0.00623 | 0.34 | 0.894 | 1.58 | 73.3 | 5.44705 |
| B | 1.0 | 2.97E−15 | 0.28389 | 0.59 | 0.37977 | 1.03 | 0.5222 | 1.56 | 0.04644 | 0.41 | 2.958 | 1.66 | 70.5 | 5.26945 |
| C | 2.0 | 4.83E−15 | 0.46124 | 0.68 | 0.80945 | 1.82 | 1.1409 | 1.91 | 0.30175 | 1.25 | 3.437 | 1.74 | 83.2 | 4.74526 |
| D | 3.0 | 9.57E−15 | 0.91352 | 0.86 | 1.67572 | 2.51 | 2.0841 | 2.12 | 0.86354 | 1.74 | 3.155 | 1.62 | 97.3 | 5.31674 |
| E | 3.5 | 8.23E−15 | 0.78615 | 1.11 | 1.42415 | 1.92 | 1.7982 | 1.93 | 0.79177 | 2.18 | 2.493 | 1.70 | 98.7 | 5.45845 |
| F | 4.0 | 1.08E−14 | 1.03031 | 0.99 | 1.84797 | 1.42 | 2.3459 | 2.22 | 1.04196 | 4.53 | 3.466 | 1.78 | 98.1 | 5.48319 |
| G | 4.5 | 1.58E−14 | 1.50503 | 1.91 | 2.68337 | 2.31 | 3.2651 | 2.45 | 1.43274 | 5.81 | 4.354 | 1.63 | 99.1 | 5.56719 |
| H | 5.0 | 1.23E−14 | 1.17480 | 0.72 | 2.10604 | 1.92 | 2.6711 | 2.45 | 1.18087 | 2.37 | 3.220 | 1.71 | 99.9 | 5.58655 |
| I | 5.5 | 1.07E−14 | 1.02511 | 1.21 | 1.82579 | 1.42 | 2.1541 | 2.54 | 1.06036 | 3.82 | 3.095 | 1.88 | 99.3 | 5.59020 |
| J | 6.0 | 9.84E−15 | 0.93946 | 0.97 | 1.66172 | 1.72 | 2.0981 | 2.51 | 0.90347 | 2.01 | 2.904 | 1.66 | 98.6 | 5.58306 |
| K | 7.0 | 1.49E−14 | 1.42628 | 1.01 | 2.52346 | 2.22 | 3.1186 | 2.79 | 1.33248 | 2.55 | 4.526 | 1.74 | 98.1 | 5.55503 |
| L | 8.0 | 1.10E−14 | 1.04627 | 1.21 | 1.86079 | 1.72 | 2.3874 | 2.15 | 1.14403 | 4.55 | 3.554 | 1.74 | 98.7 | 5.56264 |
| M | 9.0 | 1.05E−14 | 1.00506 | 1.31 | 1.79407 | 2.31 | 2.1591 | 2.49 | 1.02569 | 2.55 | 2.837 | 1.19 | 99.8 | 5.60404 |
| N | 10.0 | 6.41E−15 | 0.61219 | 1.01 | 1.09883 | 2.02 | 1.2350 | 2.22 | 0.64627 | 1.43 | 1.781 | 1.16 | 99.8 | 5.57491 |
| O | 11.0 | 5.73E−15 | 0.54674 | 0.40 | 0.98238 | 1.82 | 1.1939 | 1.87 | 0.64561 | 3.47 | 1.745 | 1.13 | 100.0 | 5.57995 |
| P | 13.0 | 1.18E−14 | 1.13165 | 1.10 | 2.03544 | 2.02 | 2.4908 | 2.57 | 1.26407 | 2.56 | 3.588 | 1.60 | 99.6 | 5.54828 |
| Q | 15.0 | 1.32E−14 | 1.25708 | 1.30 | 2.23161 | 2.32 | 2.7392 | 2.38 | 1.31670 | 5.11 | 4.075 | 1.77 | 98.8 | 5.57751 |
| R | 17.0 | 6.91E−15 | 0.65976 | 0.96 | 1.17350 | 2.12 | 1.4085 | 2.20 | 0.70525 | 1.58 | 2.325 | 1.60 | 98.1 | 5.52946 |
| S | 19.0 | 5.45E−15 | 0.52065 | 0.89 | 0.93267 | 1.72 | 1.1549 | 1.94 | 0.56381 | 1.28 | 1.599 | 1.52 | 99.6 | 5.57175 |
| T | 21.0 | 2.29E−15 | 0.21907 | 0.64 | 0.39150 | 1.23 | 0.4764 | 1.70 | 0.29765 | 1.25 | 0.818 | 1.60 | 99.8 | 5.60246 |
| U | 25.0 | 2.61E−15 | 0.24968 | 0.65 | 0.43979 | 1.13 | 0.5508 | 1.86 | 0.31461 | 1.20 | 0.895 | 1.45 | 99.5 | 5.66349 |
| V | 30.0 | 2.07E−15 | 0.19761 | 0.57 | 0.35355 | 1.13 | 0.4359 | 1.61 | 0.20480 | 0.95 | 0.745 | 1.51 | 97.1 | 5.44124 |
| W | 35.0 | 1.52E−15 | 0.14560 | 0.39 | 0.25177 | 0.87 | 0.2547 | 1.35 | 0.15352 | 0.77 | 0.719 | 1.43 | 93.8 | 5.43822 |
| X | 40.0 | 9.78E−16 | 0.09338 | 0.31 | 0.07986 | 0.67 | 0.0948 | 1.35 | 0.04472 | 0.47 | 2.090 | 1.68 | 37.6 | 4.40197 |

Plateau Age (steps E–X):

Standard: FCs — Lab #: 33019 — Age: 28.02 Ma — $D^1$: 1.0064 ± 0.0025 — Heating: 11s

Irradiation coordinates: $x = 0.53$ cm; $y = 0.85$ cm; $z = 0.31$ cm

| N | Power (W) | $^{40}$Ar (moles) | $^{40}$Ar ($10^{-9}$ A) | $\pm\sigma$ ($10^{-12}$ A) | $^{39}$Ar ($10^{-8}$ A) | $\pm\sigma$ ($10^{-12}$ A) | $^{38}$Ar ($10^{-10}$ A) | $\pm\sigma$ ($10^{-13}$ A) | $^{37}$Ar ($10^{-10}$ A) | $\pm\sigma$ ($10^{-13}$ A) | $^{36}$Ar ($10^{-13}$ A) | $\pm\sigma$ ($10^{-14}$ A) | %$^{40}$Ar* | $^{40}$Ar*/$^{39}$Ar$_K$ |
|---|---|---|---|---|---|---|---|---|---|---|---|---|---|---|
| 1 | 6 | 1.50E−13 | 14.24722 | 5.41 | 2.40864 | 8.1 | 2.90784 | 3.40 | 1.7624 | 3.6 | 2.93 | 3.83 | 99.5 | 0.587201 |
| 2 | 6 | 9.32E−14 | 8.83707 | 4.81 | 1.49479 | 6.3 | 1.79535 | 2.30 | 0.9241 | 3.6 | 0.88 | 3.18 | 99.8 | 0.588753 |
| 3 | 6 | 6.89E−13 | 6.53115 | 4.31 | 1.10531 | 6.0 | 1.34318 | 3.40 | 0.9526 | 6.0 | 1.78 | 3.64 | 99.3 | 0.585437 |
| 4 | 6 | 2.78E−13 | 26.31198 | 11.00 | 4.48005 | 16.0 | 5.39509 | 5.30 | 3.1305 | 6.0 | 2.57 | 3.70 | 99.8 | 0.584912 |
| 5 | 6 | 8.86E−14 | 8.39561 | 5.80 | 1.41043 | 6.7 | 1.69933 | 1.90 | 1.0669 | 3.3 | 4.91 | 3.51 | 98.4 | 0.584240 |

Weighted Mean $J$:

Explanations

$D^1$: Mass discrimination per AMU based on power law

$\Delta t^2$: Time interval (days) between end of irradiation and beginning of analysis

Blank Type[3]: Ave = average; LR = linear regression versus time

| Constants used | | Source |
|---|---|---|
| Atmospheric argon ratios | | |
| $(^{40}Ar/^{36}Ar)_A$ | 296.0 ± 0.74 | Nier (1950) |
| $(^{40}Ar/^{38}Ar)_A$ | 0.1880 ± 0.0001 | Nier (1950) |
| Interfering isotope production ratios | | |
| $(^{40}Ar/^{39}Ar)_K$ | (7.30 ± 0.92)E−04' | Renne et al. (2005) |
| $(^{38}Ar/^{39}Ar)_K$ | (1.22 ± 0.00)E−02 | Renne et al. (2005) |
| $(^{37}Ar/^{39}Ar)_K$ | (2.24 ± 0.16)E−04 | Renne et al. (2005) |
| $(^{39}Ar/^{37}Ar)_{Ca}$ | (6.95 ± 0.09)E−04 | Renne et al. (2005) |
| $(^{38}Ar/^{37}Ar)_{Ca}$ | (1.96 ± 0.08)E−05 | Renne et al. (2005) |
| $(^{36}Ar/^{37}Ar)_{Ca}$ | (2.65 ± 0.02)E−04 | Renne et al. (2005) |
| $(^{36}Cl/^{38}Cl)_{Cl}$ | 263 ± 2 | Renne et al. (2008) |
| Decay constants | | |
| $^{40}K\ \lambda_\epsilon$ | (5.81 ± 0.00)E−11 $a^{-1}$ | Steiger and Jäger (1977) |
| $^{40}K\ \lambda_\beta$ | (4.962 ± 0.000)E−10 $a^{-1}$ | Steiger and Jäger (1977) |
| $^{39}Ar$ | (2.58 ± 0.03)E−03 $a^{-1}$ | Stoenner et al. (1965) |
| $^{37}Ar$ | (5.4300 ± 0.0063)E−02 $a^{-1}$ | Renne and Norman (2001) |
| $^{36}Cl\ \lambda_\beta$ | (2.35 ± 0.02)E−06 $a^{-1}$ | Endt (1998) |

Quaternary Geochronology 4 (2009) 346–352

Contents lists available at ScienceDirect

Quaternary Geochronology

journal homepage: www.elsevier.com/locate/quageo

ELSEVIER

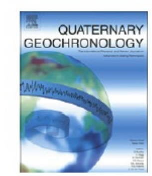


Short Communication

# Data reporting norms for $^{40}Ar/^{39}Ar$ geochronology

Paul R. Renne [a,b,*], Alan L. Deino [a], Willis E. Hames [c], Matthew T. Heizler [d], Sidney R. Hemming [e], Kip V. Hodges [f], Anthony A.P. Koppers [g], Darren F. Mark [h], Leah E. Morgan [b], David Phillips [i], Brad S. Singer [j], Brent D. Turrin [k], Igor M. Villa [l], Mike Villeneuve [m], Jan R. Wijbrans [n]

# Data reporting in $^{40}Ar/^{39}Ar$ geochronology

**Table 1**
Ar/Ar data and constants used in age calculations. All errors shown at $1\sigma$. Columns in grey are optional but recommended.

Sample: SH-10 — Lab #: 33018-23 — $J$: 0.026703 ± 0.000035 — $D^1$: 1.0066 ± 0.0028 — Heating: 60 s
Plagioclase — IGSN #: PRR001S35
Irradiation coordinates: $x$ = 0.53 cm; $y$ = 0.85 cm; $z$ = 0.31 cm

| N | Power (W) | $^{40}$Ar (moles) | $^{40}$Ar ($10^{-9}$ A) | $\pm\sigma_{40}$ ($10^{-12}$ A) | $^{39}$Ar ($10^{-10}$ A) | $\pm\sigma_{39}$ ($10^{-13}$ A) | $^{38}$Ar ($10^{-12}$ A) | $\pm\sigma_{38}$ ($10^{-14}$ A) | $^{37}$Ar ($10^{-9}$ A) | $\pm\sigma_{37}$ ($10^{-12}$ A) | $^{36}$Ar ($10^{-13}$ A) | $\pm\sigma_{36}$ ($10^{-14}$ A) | %$^{40}$Ar* | $^{40}$Ar*/$^{39}$Ar$_K$ |
|---|---|---|---|---|---|---|---|---|---|---|---|---|---|---|
| A | 0.5 | 1.02E−15 | 0.09713 | 0.43 | 0.13065 | 0.75 | 0.1826 | 1.40 | 0.00623 | 0.34 | 0.894 | 1.58 | 73.3 | 5.44705 |
| B | 1.0 | 2.97E−15 | 0.28389 | 0.59 | 0.37977 | 1.03 | 0.5222 | 1.56 | 0.04644 | 0.41 | 2.958 | 1.66 | 70.5 | 5.26945 |
| C | 2.0 | 4.83E−15 | 0.46124 | 0.68 | 0.80945 | 1.82 | 1.1409 | 1.91 | 0.30175 | 1.25 | 3.437 | 1.74 | 83.2 | 4.74526 |
| D | 3.0 | 9.57E−15 | 0.91352 | 0.86 | 1.67572 | 2.51 | 2.0841 | 2.12 | 0.86354 | 1.74 | 3.155 | 1.62 | 97.3 | 5.31674 |
| E | 3.5 | 8.23E−15 | 0.78615 | 1.11 | 1.42415 | 1.92 | 1.7982 | 1.93 | 0.79177 | 2.18 | 2.493 | 1.70 | 98.7 | 5.45845 |
| F | 4.0 | 1.08E−14 | 1.03031 | 0.99 | 1.84797 | 1.42 | 2.3459 | 2.22 | 1.04196 | 4.53 | 3.466 | 1.78 | 98.1 | 5.48319 |
| G | 4.5 | 1.58E−14 | 1.50503 | 1.91 | 2.68337 | 2.31 | 3.2651 | 2.45 | 1.43274 | 5.81 | 4.354 | 1.63 | 99.1 | 5.56719 |
| H | 5.0 | 1.23E−14 | 1.17480 | 0.72 | 2.10604 | 1.92 | 2.6711 | 2.45 | 1.18087 | 2.37 | 3.220 | 1.71 | 99.9 | 5.58655 |
| I | 5.5 | 1.07E−14 | 1.02511 | 1.21 | 1.82579 | 1.42 | 2.1541 | 2.54 | 1.06036 | 3.82 | 3.095 | 1.88 | 99.3 | 5.59020 |
| J | 6.0 | 9.84E−15 | 0.93946 | 0.97 | 1.66172 | 1.72 | 2.0981 | 2.51 | 0.90347 | 2.01 | 2.904 | 1.66 | 98.6 | 5.58306 |
| K | 7.0 | 1.49E−14 | 1.42628 | 1.01 | 2.52346 | 2.22 | 3.1186 | 2.79 | 1.33248 | 2.55 | 4.526 | 1.74 | 98.1 | 5.55503 |
| L | 8.0 | 1.10E−14 | 1.04627 | 1.21 | 1.86079 | 1.72 | 2.3874 | 2.15 | 1.14403 | 4.55 | 3.554 | 1.74 | 98.7 | 5.56264 |
| M | 9.0 | 1.05E−14 | 1.00506 | 1.31 | 1.79407 | 2.31 | 2.1591 | 2.49 | 1.02569 | 2.55 | 2.837 | 1.19 | 99.8 | 5.60404 |
| N | 10.0 | 6.41E−15 | 0.61219 | 1.01 | 1.09883 | 2.02 | 1.2350 | 2.22 | 0.64627 | 1.43 | 1.781 | 1.16 | 99.8 | 5.57491 |
| O | 11.0 | 5.73E−15 | 0.54674 | 0.40 | 0.98238 | 1.82 | 1.1939 | 1.87 | 0.64561 | 3.47 | 1.745 | 1.13 | 100.0 | 5.57995 |
| P | 13.0 | 1.18E−14 | 1.13165 | 1.10 | 2.03544 | 2.02 | 2.4908 | 2.57 | 1.26407 | 2.56 | 3.588 | 1.60 | 99.6 | 5.54828 |
| Q | 15.0 | 1.32E−14 | 1.25708 | 1.30 | 2.23161 | 2.32 | 2.7392 | 2.38 | 1.31670 | 5.11 | 4.075 | 1.77 | 98.8 | 5.57751 |
| R | 17.0 | 6.91E−15 | 0.65976 | 0.96 | 1.17350 | 2.12 | 1.4085 | 2.20 | 0.70525 | 1.58 | 2.325 | 1.60 | 98.1 | 5.52946 |
| S | 19.0 | 5.45E−15 | 0.52065 | 0.89 | 0.93267 | 1.72 | 1.1549 | 1.94 | 0.56381 | 1.28 | 1.599 | 1.52 | 99.6 | 5.57175 |
| T | 21.0 | 2.29E−15 | 0.21907 | 0.64 | 0.39150 | 1.23 | 0.4764 | 1.70 | 0.29765 | 1.25 | 0.818 | 1.60 | 99.8 | 5.60246 |
| U | 25.0 | 2.61E−15 | 0.24968 | 0.65 | 0.43979 | 1.13 | 0.5508 | 1.86 | 0.31461 | 1.20 | 0.895 | 1.45 | 99.5 | 5.66349 |
| V | 30.0 | 2.07E−15 | 0.19761 | 0.57 | 0.35355 | 1.13 | 0.4359 | 1.61 | 0.20480 | 0.95 | 0.745 | 1.51 | 97.1 | 5.44124 |
| W | 35.0 | 1.52E−15 | 0.14560 | 0.39 | 0.25177 | 0.87 | 0.2547 | 1.35 | 0.15352 | 0.77 | 0.719 | 1.43 | 93.8 | 5.43822 |
| X | 40.0 | 9.78E−16 | 0.09338 | 0.31 | 0.07986 | 0.67 | 0.0948 | 1.35 | 0.04472 | 0.47 | 2.090 | 1.68 | 37.6 | 4.40197 |

Heating: 60 s
IGSN #: PRR001S35
Irradiation coordinates: $x$ = 0.53 cm; $y$ = 0.85 cm; $z$ = 0.31 cm — Background Correction

| N | $\pm\sigma$ | Age (Ma) | $\pm\sigma$ (Ma) | Ca/K | $\Delta t^2$ (days) | Blank type[3] | $^{40}$Ar ($10^{-12}$ A) | $\pm\sigma_{40}$ ($10^{-14}$ A) | $^{39}$Ar ($10^{-14}$ A) | $\pm\sigma_{39}$ ($10^{-15}$ A) | $^{38}$Ar ($10^{-15}$ A) | $\pm\sigma_{38}$ ($10^{-16}$ A) | $^{37}$Ar ($10^{-15}$ A) | $\pm\sigma_{37}$ ($10^{-16}$ A) | $^{36}$Ar ($10^{-15}$ A) | $\pm\sigma_{36}$ ($10^{-16}$ A) |
|---|---|---|---|---|---|---|---|---|---|---|---|---|---|---|---|---|
| A | 0.33890 | 244.99 | 15.24 | 0.94 | 146.50 | LR | 3.81130 | 1.906 | 1.511 | 1.21 | 1.82 | 1.6 | 4.30 | 0.8 | 3.70 | 0.6 |
| B | 0.12829 | 237.51 | 5.78 | 2.40 | 146.52 | LR | 3.81062 | 1.905 | 1.511 | 1.21 | 1.82 | 1.6 | 4.30 | 0.8 | 3.70 | 0.6 |
| C | 0.06661 | 215.23 | 3.02 | 7.31 | 146.55 | LR | 3.80924 | 1.905 | 1.510 | 1.21 | 1.81 | 1.6 | 4.30 | 0.8 | 3.70 | 0.6 |
| D | 0.03604 | 239.50 | 1.62 | 10.10 | 146.60 | LR | 3.80649 | 1.903 | 1.509 | 1.21 | 1.81 | 1.6 | 4.29 | 0.8 | 3.70 | 0.6 |
| E | 0.04152 | 245.47 | 1.87 | 10.90 | 146.63 | LR | 3.80302 | 1.902 | 1.508 | 1.21 | 1.81 | 1.6 | 4.29 | 0.8 | 3.69 | 0.6 |
| F | 0.03607 | 246.51 | 1.62 | 11.05 | 146.66 | LR | 3.79885 | 1.899 | 1.506 | 1.20 | 1.81 | 1.6 | 4.29 | 0.8 | 3.69 | 0.6 |
| G | 0.02921 | 250.04 | 1.31 | 10.47 | 146.71 | LR | 3.79333 | 1.897 | 1.504 | 1.20 | 1.81 | 1.6 | 4.28 | 0.8 | 3.68 | 0.6 |
| H | 0.03244 | 250.85 | 1.46 | 10.99 | 146.74 | LR | 3.78713 | 1.894 | 1.501 | 1.20 | 1.80 | 1.6 | 4.27 | 0.8 | 3.68 | 0.6 |
| I | 0.03766 | 251.00 | 1.69 | 11.38 | 146.76 | LR | 3.78026 | 1.890 | 1.499 | 1.20 | 1.80 | 1.6 | 4.26 | 0.8 | 3.67 | 0.6 |
| J | 0.03672 | 250.70 | 1.65 | 10.66 | 146.82 | LR | 3.77205 | 1.886 | 1.495 | 1.20 | 1.80 | 1.6 | 4.26 | 0.8 | 3.66 | 0.5 |
| K | 0.03023 | 249.53 | 1.36 | 10.35 | 146.84 | LR | 3.76316 | 1.882 | 1.492 | 1.19 | 1.79 | 1.6 | 4.25 | 0.8 | 3.65 | 0.5 |
| L | 0.03646 | 249.85 | 1.64 | 12.05 | 146.87 | LR | 3.75360 | 1.877 | 1.488 | 1.19 | 1.79 | 1.6 | 4.23 | 0.8 | 3.64 | 0.5 |
| M | 0.03102 | 251.58 | 1.39 | 11.21 | 146.92 | LR | 3.74277 | 1.871 | 1.484 | 1.19 | 1.78 | 1.6 | 4.22 | 0.8 | 3.63 | 0.5 |
| N | 0.03965 | 250.36 | 1.78 | 11.53 | 146.95 | LR | 3.73127 | 1.866 | 1.479 | 1.18 | 1.78 | 1.6 | 4.21 | 0.8 | 3.62 | 0.5 |
| O | 0.04189 | 250.57 | 1.88 | 12.88 | 146.98 | LR | 3.71910 | 1.860 | 1.474 | 1.18 | 1.77 | 1.6 | 4.20 | 0.8 | 3.61 | 0.5 |
| P | 0.03334 | 249.25 | 1.50 | 12.17 | 147.03 | LR | 3.70566 | 1.853 | 1.469 | 1.18 | 1.77 | 1.6 | 4.18 | 0.8 | 3.60 | 0.5 |
| Q | 0.03334 | 250.47 | 1.50 | 11.56 | 147.06 | LR | 3.69160 | 1.846 | 1.463 | 1.17 | 1.76 | 1.6 | 4.16 | 0.8 | 3.58 | 0.5 |
| R | 0.04655 | 248.46 | 2.09 | 11.78 | 147.08 | LR | 3.67693 | 1.838 | 1.458 | 1.17 | 1.75 | 1.6 | 4.15 | 0.8 | 3.57 | 0.5 |
| S | 0.05278 | 250.23 | 2.37 | 11.85 | 147.13 | LR | 3.66101 | 1.831 | 1.451 | 1.16 | 1.74 | 1.6 | 4.13 | 0.8 | 3.55 | 0.5 |
| T | 0.11888 | 251.52 | 5.34 | 14.90 | 147.16 | LR | 3.64448 | 1.822 | 1.445 | 1.16 | 1.74 | 1.6 | 4.11 | 0.8 | 3.54 | 0.5 |
| U | 0.09719 | 254.07 | 4.36 | 14.02 | 147.19 | LR | 3.62735 | 1.814 | 1.438 | 1.15 | 1.73 | 1.6 | 4.09 | 0.8 | 3.52 | 0.5 |
| V | 0.12304 | 244.75 | 5.53 | 11.35 | 147.24 | LR | 3.60903 | 1.805 | 1.431 | 1.14 | 1.72 | 1.5 | 4.07 | 0.8 | 3.50 | 0.5 |
| W | 0.16149 | 244.62 | 7.26 | 11.95 | 147.27 | LR | 3.59014 | 1.795 | 1.423 | 1.14 | 1.71 | 1.5 | 4.05 | 0.8 | 3.49 | 0.5 |
| X | 0.60000 | 200.50 | 27.33 | 10.98 | 147.29 | LR | 3.57072 | 1.785 | 1.416 | 1.13 | 1.70 | 1.5 | 4.03 | 0.8 | 3.47 | 0.5 |
| Plateau Age (steps E–X): | | **249.78** | **0.49** | | | | | | | | | | | | | |

Standard: FCs — Lab #: 33019 — Age: 28.02 Ma — $D^1$: 1.0064 ± 0.0025 — Heating: 11s
Irradiation coordinates: $x$ = 0.53 cm; $y$ = 0.85 cm; $z$ = 0.31 cm

| N | Power (W) | $^{40}$Ar (moles) | $^{40}$Ar ($10^{-9}$ A) | $\pm\sigma$ ($10^{-12}$ A) | $^{39}$Ar ($10^{-8}$ A) | $\pm\sigma$ ($10^{-12}$ A) | $^{38}$Ar ($10^{-10}$ A) | $\pm\sigma$ ($10^{-13}$ A) | $^{37}$Ar ($10^{-10}$ A) | $\pm\sigma$ ($10^{-13}$ A) | $^{36}$Ar ($10^{-13}$ A) | $\pm\sigma$ ($10^{-14}$ A) | %$^{40}$Ar* | $^{40}$Ar*/$^{39}$Ar$_K$ |
|---|---|---|---|---|---|---|---|---|---|---|---|---|---|---|
| 1 | 6 | 1.50E−13 | 14.24722 | 5.41 | 2.40864 | 8.1 | 2.90784 | 3.40 | 1.7624 | 3.6 | 2.93 | 3.83 | 99.5 | 0.587201 |
| 2 | 6 | 9.32E−14 | 8.83707 | 4.81 | 1.49479 | 6.3 | 1.79535 | 2.30 | 0.9241 | 3.6 | 0.88 | 3.18 | 99.8 | 0.588753 |
| 3 | 6 | 6.89E−14 | 6.53115 | 4.31 | 1.10531 | 6.0 | 1.34318 | 3.40 | 0.9526 | 6.0 | 1.78 | 3.64 | 99.3 | 0.585437 |
| 4 | 6 | 2.78E−13 | 26.31198 | 11.00 | 4.48005 | 16.0 | 5.39509 | 5.30 | 3.1305 | 6.0 | 2.57 | 3.70 | 99.8 | 0.584912 |
| 5 | 6 | 8.86E−14 | 8.39561 | 5.80 | 1.41043 | 6.7 | 1.69933 | 1.90 | 1.0669 | 3.3 | 4.91 | 3.51 | 98.4 | 0.584240 |

Background Correction

| N | $\pm\sigma$ | $J$ | $\pm\sigma$ | Ca/K | $\Delta t^2$ (days) | Blank type[3] | $^{40}$Ar ($10^{-12}$ A) | $\pm\sigma$ ($10^{-14}$ A) | $^{39}$Ar ($10^{-13}$ A) | $\pm\sigma$ ($10^{-15}$ A) | $^{38}$Ar ($10^{-15}$ A) | $\pm\sigma$ ($10^{-16}$ A) | $^{37}$Ar ($10^{-15}$ A) | $\pm\sigma$ ($10^{-16}$ A) | $^{36}$Ar ($10^{-15}$ A) | $\pm\sigma$ ($10^{-16}$ A) |
|---|---|---|---|---|---|---|---|---|---|---|---|---|---|---|---|---|
| 1 | 0.001619 | 0.026657 | 0.000073 | 0.014 | 70.05 | Ave | 7.59623 | 3.136 | 5.4374 | 4.38 | 2.90784 | 3.40 | 3.71 | 0.5 | 5.07 | 0.7 |
| 2 | 0.001683 | 0.026586 | 0.000076 | 0.012 | 70.08 | Ave | 7.59623 | 3.136 | 5.4374 | 4.38 | 1.79535 | 3.40 | 3.71 | 0.5 | 5.07 | 0.7 |
| 3 | 0.001880 | 0.026737 | 0.000086 | 0.017 | 70.10 | Ave | 7.59623 | 3.136 | 5.4374 | 4.38 | 1.34318 | 3.40 | 3.71 | 0.5 | 5.07 | 0.7 |
| 4 | 0.001550 | 0.026761 | 0.000071 | 0.014 | 70.16 | Ave | 7.59623 | 3.136 | 5.4374 | 4.38 | 5.39509 | 3.40 | 3.71 | 0.5 | 5.07 | 0.7 |
| 5 | 0.001812 | 0.026792 | 0.000083 | 0.015 | 70.18 | Ave | 7.59623 | 3.136 | 5.4374 | 4.38 | 1.69933 | 3.40 | 3.71 | 0.5 | 5.07 | 0.7 |
| Weighted Mean $J$: | | **0.026703** | **0.000035** | | | | | | | | | | | | | |

Explanations
$D^1$: Mass discrimination per AMU based on power law
$\Delta t^2$: Time interval (days) between end of irradiation and beginning of analysis
Blank Type[3]: Ave = average; LR = linear regression versus time

| Constants used | | Source |
|---|---|---|
| Atmospheric argon ratios | | |
| $(^{40}Ar/^{36}Ar)_A$ | 296.0 ± 0.74 | Nier (1950) |
| $(^{40}Ar/^{38}Ar)_A$ | 0.1880 ± 0.0001 | Nier (1950) |
| Interfering isotope production ratios | | |
| $(^{40}Ar/^{39}Ar)_K$ | (7.30 ± 0.92)E−04' | Renne et al. (2005) |
| $(^{38}Ar/^{39}Ar)_K$ | (1.22 ± 0.00)E−02 | Renne et al. (2005) |
| $(^{37}Ar/^{39}Ar)_K$ | (2.24 ± 0.16)E−04 | Renne et al. (2005) |
| $(^{39}Ar/^{37}Ar)_{Ca}$ | (6.95 ± 0.09)E−04 | Renne et al. (2005) |
| $(^{38}Ar/^{37}Ar)_{Ca}$ | (1.96 ± 0.08)E−05 | Renne et al. (2005) |
| $(^{36}Ar/^{37}Ar)_{Ca}$ | (2.65 ± 0.02)E−04 | Renne et al. (2005) |
| $(^{36}Cl/^{38}Cl)_{Cl}$ | 263 ± 2 | Renne et al. (2008) |
| Decay constants | | |
| $^{40}K\ \lambda_\epsilon$ | (5.81 ± 0.00)E−11 $a^{-1}$ | Steiger and Jäger (1977) |
| $^{40}K\ \lambda_\beta$ | (4.962 ± 0.000)E−10 $a^{-1}$ | Steiger and Jäger (1977) |
| $^{39}Ar$ | (2.58 ± 0.03)E−03 $a^{-1}$ | Stoenner et al. (1965) |
| $^{37}Ar$ | (5.4300 ± 0.0063)E−02 $a^{-1}$ | Renne and Norman (2001) |
| $^{36}Cl\ \lambda_\beta$ | (2.35 ± 0.02)E−06 $a^{-1}$ | Endt (1998) |

Quaternary Geochronology 4 (2009) 346–352

Contents lists available at ScienceDirect

Quaternary Geochronology

journal homepage: www.elsevier.com/locate/quageo

ELSEVIER

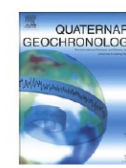


Short Communication

## Data reporting norms for $^{40}Ar/^{39}Ar$ geochronology

Paul R. Renne[a,b,*], Alan L. Deino[a], Willis E. Hames[c], Matthew T. Heizler[d], Sidney R. Hemming[e], Kip V. Hodges[f], Anthony A.P. Koppers[g], Darren F. Mark[h], Leah E. Morgan[b], David Phillips[i], Brad S. Singer[j], Brent D. Turrin[k], Igor M. Villa[l], Mike Villeneuve[m], Jan R. Wijbrans[n]

# Systematic errors and total uncertainty

- With high precision dating, must consider sources of internal error (analytical, J), as well as external error (decay constant, standard age)
- Karner and Renne (1998), Renne et al. (1998); combine all systematic sources of error quadratically

variance of age t | variance of $\lambda_e$ | variance of $\lambda_B$ | variance fluence monitor | variance R (intercalibration factor)

$$\sigma_t^2 = \left(\frac{\partial t}{\partial \lambda_e}\right)^2 \sigma_{\lambda e}^2 + \left(\frac{\partial t}{\partial \lambda_\beta}\right)^2 \sigma_{\lambda\beta}^2 + \left(\frac{\partial t}{\partial K}\right)^2 \sigma_K^2 + \left(\frac{\partial t}{\partial R}\right)^2 \sigma_R^2$$

where:

$$K = \left(\frac{{}^{40}Ar^*}{{}^{39}Ar_K}\right)_s \qquad R = \frac{\left(\frac{{}^{40}Ar^*}{{}^{39}Ar_K}\right)_u}{\left(\frac{{}^{40}Ar^*}{{}^{39}Ar_K}\right)_s}$$

$$\sigma_R^2 = \left(\frac{\sigma_{r_u}}{r_s}\right)^2 + \left(\frac{r_u \sigma_{r_s}}{r_s^2}\right)^2$$

$$\sigma_t^2 = \left\{\frac{1}{\lambda}\left(t + \frac{\lambda_\beta KR}{\lambda_e^2 \exp(\lambda t)}\right)\right\}^2 \sigma_{\lambda e}^2 + \left\{\frac{1}{\lambda}\left(t + \frac{KR}{\lambda_e \exp(\lambda t)} - t\right)\right\}^2 \sigma_{\lambda\beta}^2 + \left\{\frac{R}{\lambda_e \exp(\lambda t)}\right\}^2 \sigma_K^2 + \left\{\frac{KR}{R\lambda_e \exp(\lambda t)}\right\}^2 \sigma_R^2$$

# Preferred ages for $^{40}Ar/^{39}Ar$ standard minerals

- **GTS2012 values**
- **Reference is astronomically calibrated age of FCs (Kuiper et al., 2008)**

TABLE 6.1 Preferred Ages of $^{40}Ar/^{39}Ar$ Standards Utilized in GTS2012

| Standard Name | Intercalibration Factor ($R^{i}_{FCs}$) | Apparent Age* ± int. (ext.) (Ma) | References |
|---|---|---|---|
| FCs, FCT-3 | | 28.201 ± (0.046) | Kuiper et al. (2008) |
| MMhb-1 | 21.4876 ± 0.0079 | 527.0 ± 0.3 (2.6) | Renne et al. (1998) |
| Hb3gr | 51.8780 ± 0.0754 | 1081.5 ± 2.4 (10.4) | Jourdan and Renne (2007); Jourdan et al. (2006) |
| TCs | 1.0112 ± 0.0010 | 28.51 ± 0.06 (0.06) | Renne et al. (1998) |
| GA-1550 | 3.5958 ± 0.0031 | 99.44 ± 0.17 (0.18) | Jourdan and Renne (2007); Renne et al. (1998b) |
| ACs | 0.04229 ± 0.00006 | 1.201 ± 0.003 (0.003) | Renne et al. (1998) |
| GHC-305 | 3.8540 ± 0.0128 | 106.4 ± 0.7 (0.7) | Jourdan and Renne (2007); Renne et al. (1998) |
| LP-6 | 4.6654 ± 0.0058 | 128.0 ± 0.3 (0.3) | Baksi et al. (1996) |
| Bern 4 Mu | 0.6606 ± 0.0053 | 18.68 ± 0.30 (0.30) | Baksi et al. (1996) |
| Bern 4 Bi | 0.6138 ± 0.0050 | 17.36 ± 0.28 (0.28) | Baksi et al. (1996) |
| SB-3 | 6.0582 ± 0.0249 | 164.5 ± 1.3 (1.3) | Baksi et al. (1996) |

*All ages are referenced to Fish Canyon Tuff sanidine (FCs) 28.201 Ma.

*Schmitz (2012)*

# Flow chart & time line for $^{40}Ar/^{39}Ar$ analyes in WiscAr lab

## Outcrop


## Sample preparation

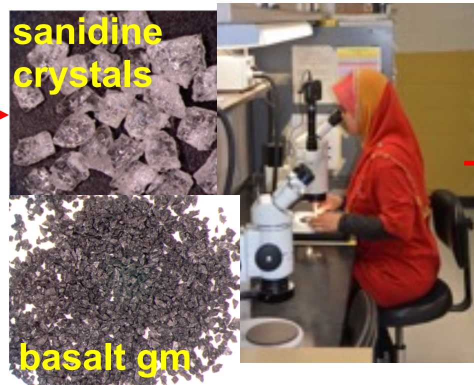


## Irradiation

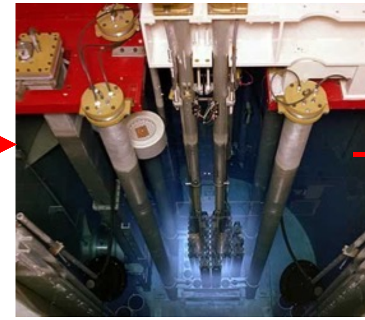

## Degassing, mass spectrometry

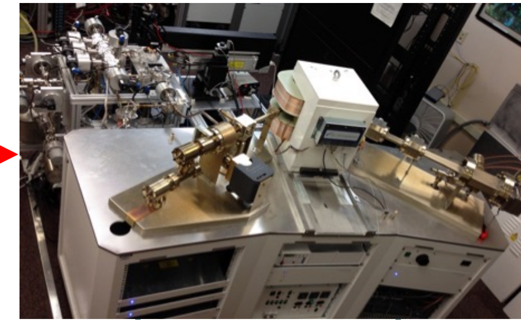

*Timeline:* *Weeks*

*Weeks*

*2-3 month queue*
*cooldown in lab 2+ mo.*


| Standard mineral | Sanidine |
|---|---|
| Standard gas | Standard gas |
| Blank | Blank |
| $J$ value | $F$ value |

$$t = \frac{1}{\lambda} ln\left[1 + J\left(\frac{^{40}Ar^*}{^{39}Ar_K}\right)\right]$$

*1 hour each set of measurements*

*12 hours for one incremental heating analysis*

## Plotting, interrogation, interpretation

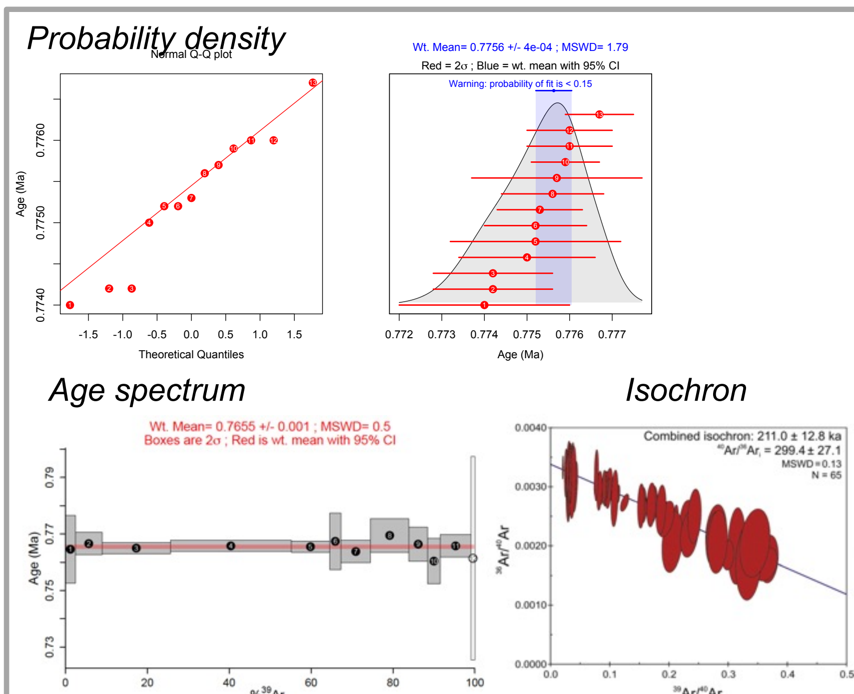


*Days to weeks*

# $^{40}Ar/^{39}Ar$ Geochronology

- Basic issues and assumptions, nomenclature, age equation
- $^{40}Ar/^{39}Ar$ dating in practice
  - gas extraction
  - irradiation, undesirable nuclear reactions and their corrections
  - multi-collector mass spectrometry – ***a revolution***
  - minimizing uncertainties
  - appropriate samples
- Reporting, presentation, and interpretation of complex data sets
  - metadata, age spectrum, isochron, probability/kernal density, rank-order plots
  - evaluation of FCs & ACs standard ages and homogeneity
  - why precision matters and what do dates record?
  - examples: the Bishop Tuff & future challenges
- Calculation of apparent ages and uncertainties
  - standard minerals used to monitor neutron fluence
  - GTS2012 calibrates $^{40}Ar/^{39}Ar$ ages to 28.201 $\pm$ 0.046 Ma Fish Canyon sanidine (FCs) [Kuiper et al., 2008, astronomical basis]
  - Alder Creek sanidine now calibrated to 1.1864 $\pm$ 0.0006 Ma [Jicha et al., 2016]
  - analytical + systematic [decay constant & standard age] uncertainties
- Recalibrating published (legacy) dates [Mercer & Hodges, 2016]

WiscAr

# Data Reporting and Interpretation

Four main ways to portray results:

**Age spectrum diagrams**

- Error-weighted mean 'plateau' ages

**Isotope correlation (isochron) diagrams**

- Regression analysis
- Inverse isochron diagrams

**Simple 'rank order' diagrams for comparing among data sets**

**Probability density or Kernal density diagrams**

# Age spectrum diagrams

*Sharp & Renne (2005)*
*Mauna Kea alkali basalt*

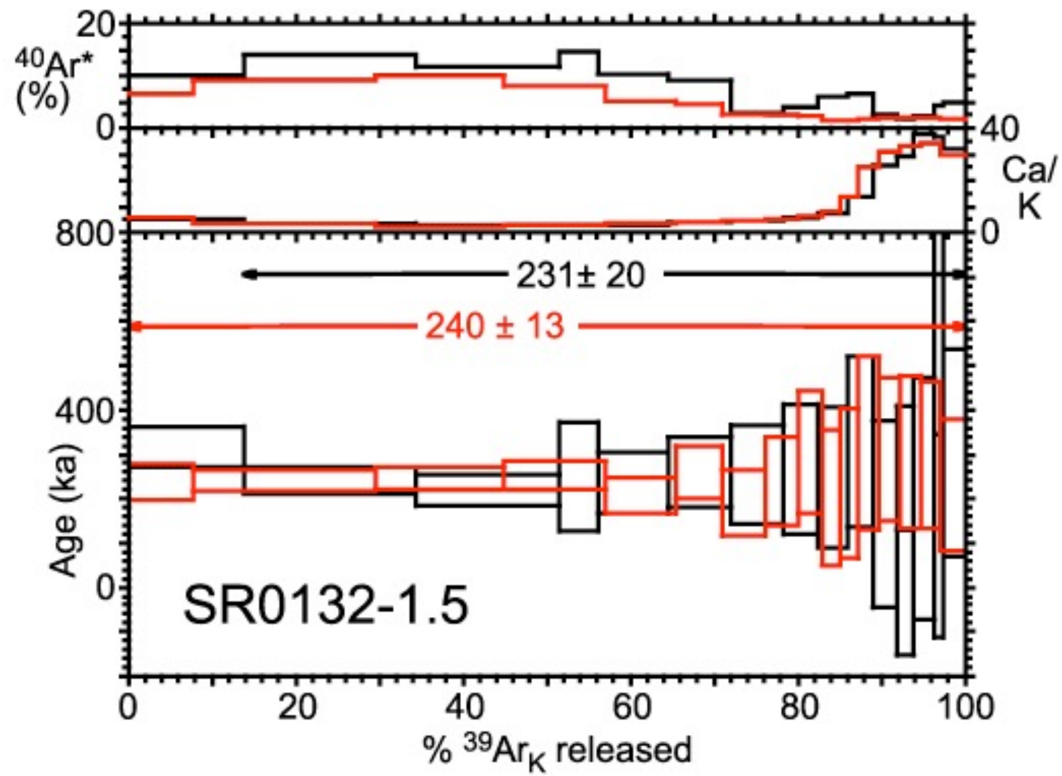


## Plot apparent ages ± uncertainty vs. % $^{39}Ar$ released

- *K/Ca spectrum*
    - *mineral control on release pattern*
- *Spectrum of radiogenic $^{40}Ar^*$*
    - *indicator of Ar loss; air contamination*

## For rocks with simple thermal history, define "plateau" age

- *Arbitrary criteria (e.g., Fleck et al., 1977); three consecutive steps, concordant in age at 95% confidence level, comprising > 50% of gas released*

# Age spectrum diagrams

*Sharp & Renne (2005)*
*Mauna Kea alkali basalt*

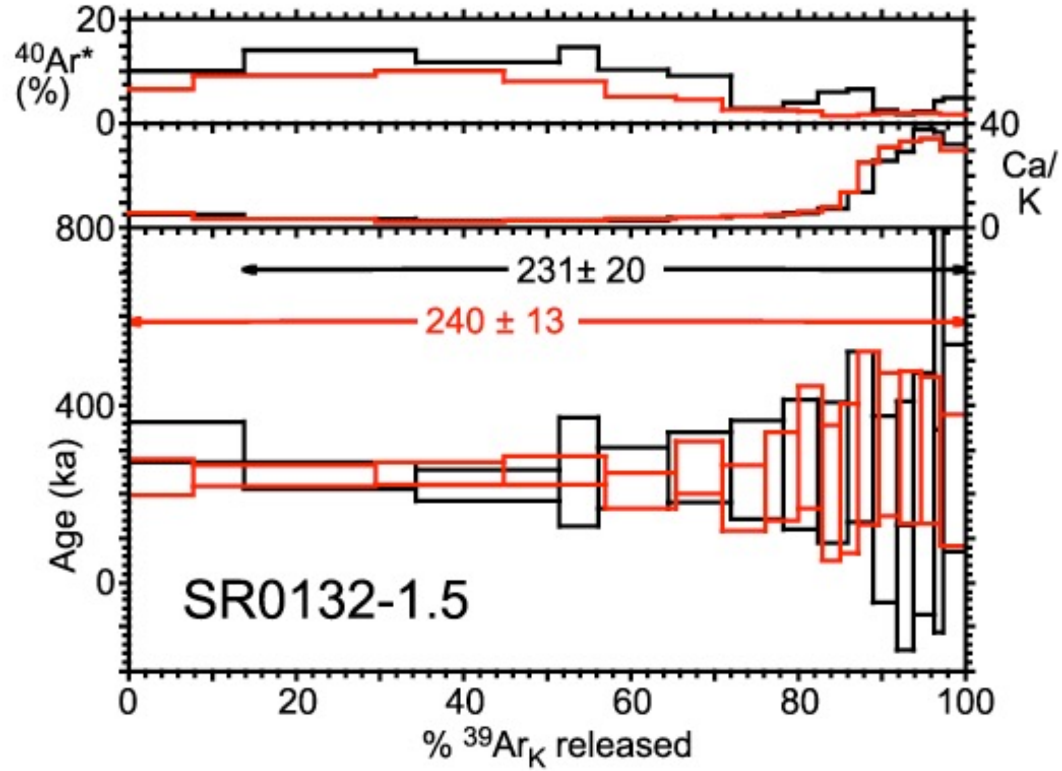


**Each apparent age/step weighted by inverse of variance, $1/\sigma_i^2$**

- *gives much less weight to steps with larger uncertainties*
- *inverse-variance weighted mean* $x_{best} = \Sigma w_i x_i / \Sigma w_i$
- *where weights are* $w_i = 1/\sigma_i^2$ $x_i$ = *individual measured ages*
- *error estimate for weighted mean* $\sigma_{xbest} = (\Sigma w_i)^{-1/2}$

# Age spectrum diagrams

*Sharp & Renne (2005)*
*Mauna Kea alkali basalt*

**Statistical evaluation of the best-fit solution**

How do we evaluate how well a best-fit solution, in this case the weighted mean of a normal distribution, describes our data distribution?

We can define our goodness-of-fit parameter, $\chi^2$, as the sum of the squares of the deviations of our observations from our model mean value, weighted by the variances of those observations:

$$\chi^2 = \sum_{i=1}^{n} \left( \frac{x_i - \bar{x}}{\sigma_i} \right)^2$$

In geochronology, we have a tradition of normalizing the $\chi^2$ statistic by the degrees of freedom of the system to derive the **Mean Squared Weighted Deviation** or **MSWD** (e.g. Wendt and Carl, 1991). This statistic quantifies the extent to which data scatter from the best-fit solution beyond stated uncertainties.

$$MSWD = \frac{\chi^2}{f} = \frac{\chi^2}{n-1}$$

$f$ is the degrees of freedom of the model, e.g. the number of experimental parameters (measurements) – number of model parameters (unknowns)

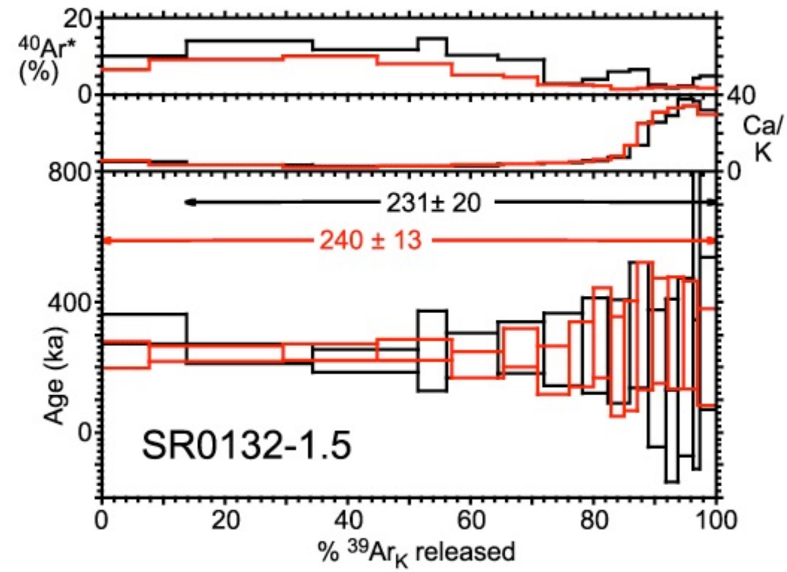


*MSWD=0.28; 86% of $^{39}$Ar*
*MSWD=0.81; 99% of $^{39}$Ar*

- **MSWD <1** if observed scatter is less than that predicted by analytical uncertainties. In this case, the data are said to be "underdispersed", indicating analytical uncertainties are overestimated
- **If MSWD ≈ 1**, agreement between expected and observed distribution of errors is good. This is a univariate, Gaussian, distribution. **use $\sigma_{xbest}$ as calculated**
- **If MSWD >1** if the observed scatter exceeds that predicted by the analytical uncertainties. Data are "overdispersed". If MSWD < cut-off value (students-t table), then:
  - **multiply $\sigma_{xbest}$ by (MSWD)$^{1/2}$** to obtain uncertainty estimate
- **If MSWD > cut-off value, reject plateau age**

WiscAr

# Inverse isochron diagrams

- $^{36}Ar/^{40}Ar$ vs. $^{39}Ar/^{40}Ar$
- 3-component mixing diagram
  - *radiogenic component along abcissa*
  - *trapped component along ordinate*
  - *extraneous argon below mixing line*
- isochrons make no assumption about the composition of the trapped component
  - errors more conservative than plateau errors
  - Error-weighting and MSWD criteria used to estimate goodness of fit
  - **regression may indicate excess argon as a $^{40}Ar/^{36}Ar$ intercept > 298.6**
- **spread in data below isochron may indicate inherited argon**
  - range of partly degassed radiogenic components?
  - single largely undegassed radiogenic component?

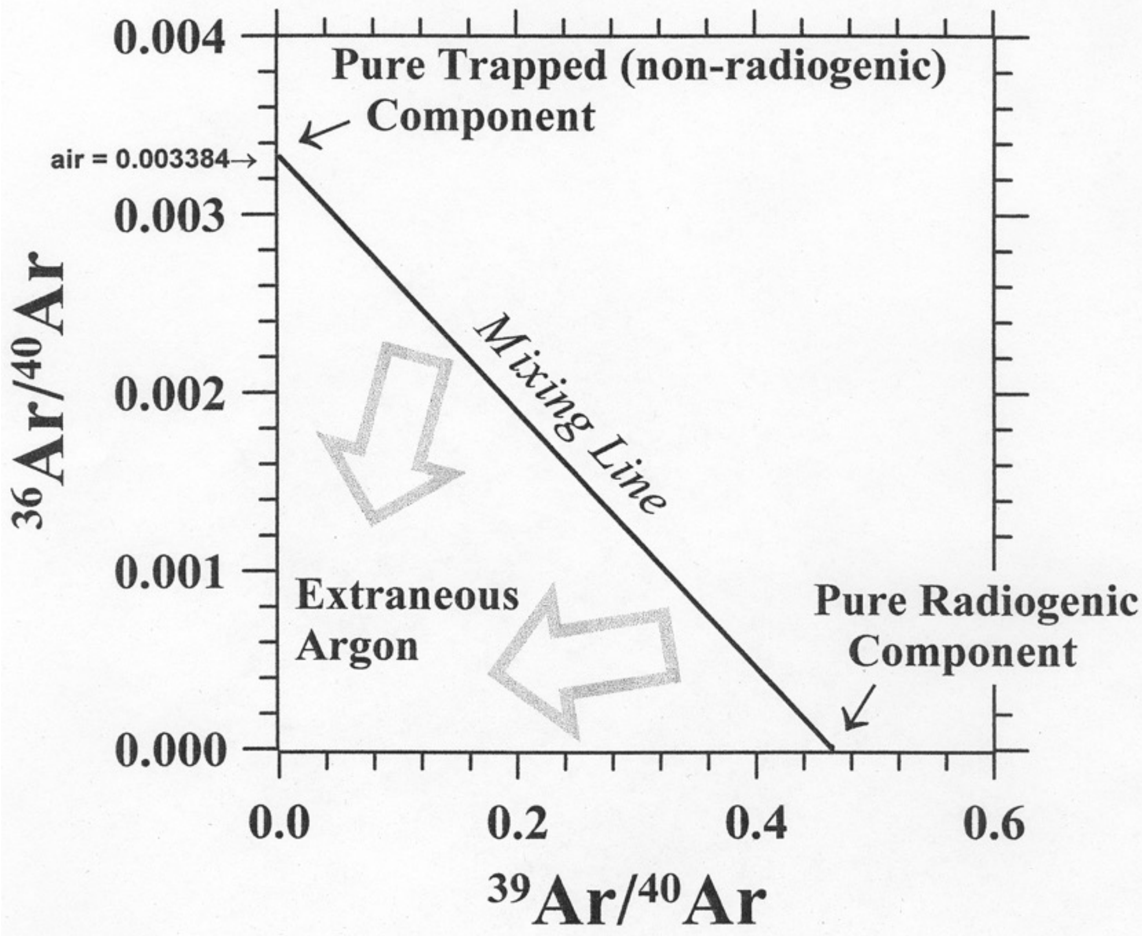


$$\leftarrow \quad t = \frac{1}{\lambda} \ln\left[1 + J\,\frac{^{40}Ar^*}{^{39}Ar_K}\right]$$

# Inverse isochron diagrams



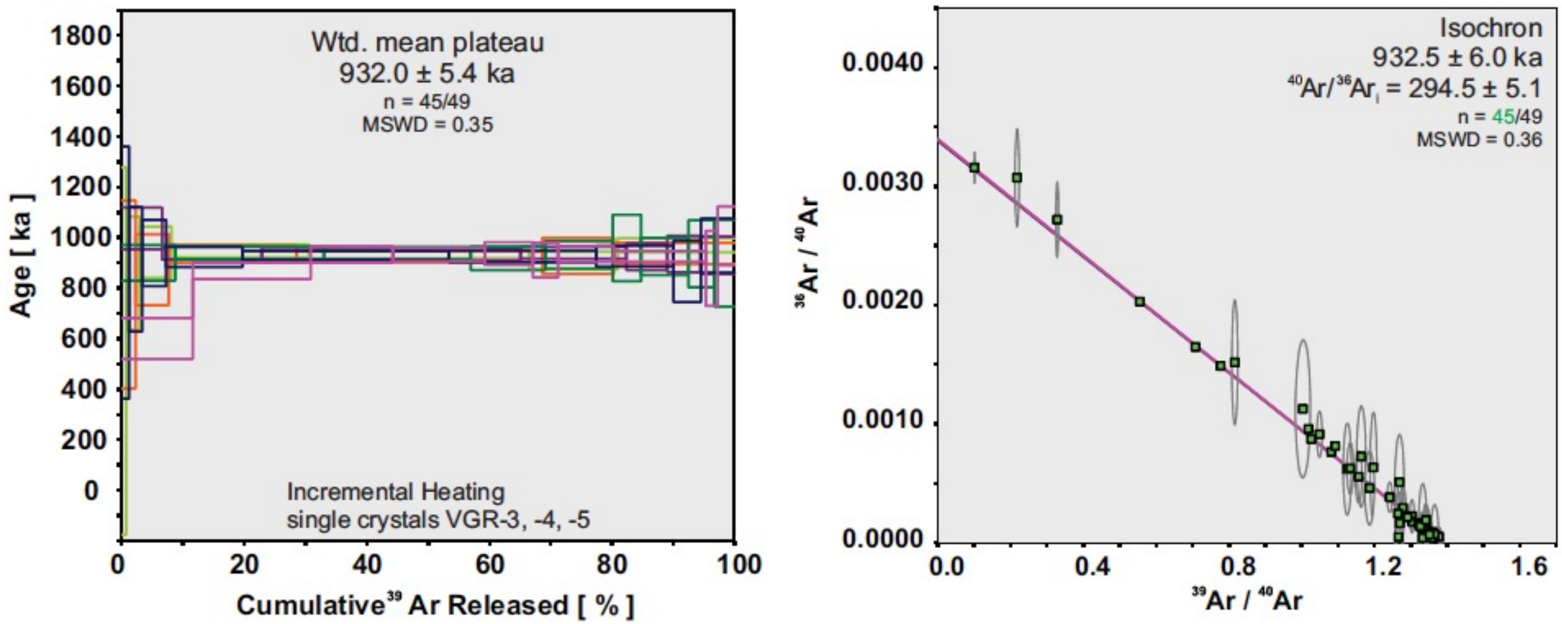


**Fig. 6.** Age spectrum and inverse isochron diagrams of laser incremental heating data from experiments on each of six large sanidine phenocrysts from sample VGR-3 (Singer and Brown, 2002) in the transitionally magnetized Cerro Santa Rosa I rhyolite dome, New Mexico. Ages obtained in 2013 at the University of Wisconsin-Madison and calculated relative to 28.201 Ma FCs (data in Supplementary documents).

## Common practice

- *regress data that define plateau segments of age spectra from incremental heating analysis*

- *Single crystal laser fusion data from sanidine can be regressed*

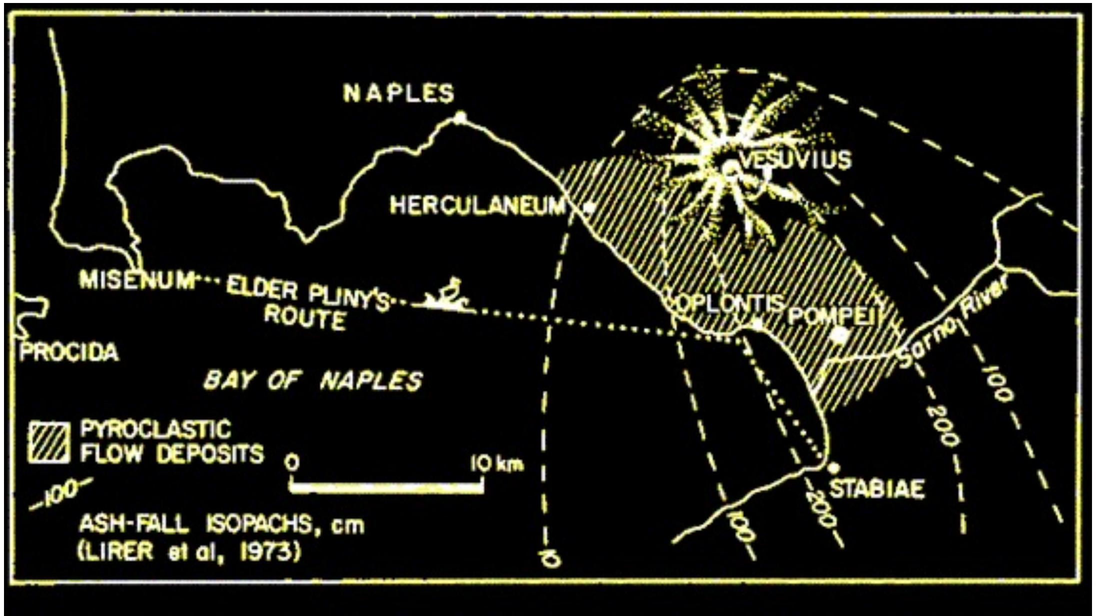


Ill. 1. Map of the Vesuvius region and Bay of Naples, showing the extent of the area affected by pyroclastic flows during the eruption of A.D. 79. Broken lines are isopachs of the pumice fall during the Plinian phase

# Excess argon in 79 A.D. Vesuvius tephra

*Renne, Sharp, Deino, Orsi, Civetta (1997) Science, v. 277*

**Fig. 1.** Isotope correlation diagram showing isochron obtained by regression of 46 analyses. The inset shows detail of 13 analyses with the lowest $^{39}Ar/^{40}Ar$. The mean of five olivine analyses is shown on the $^{36}Ar/^{40}Ar$ axis of the inset with error bars, labeled OL. OL data are not included in the regression. Trapped component [$(^{40}Ar/^{36}Ar)i$] is shown by bold arrow.

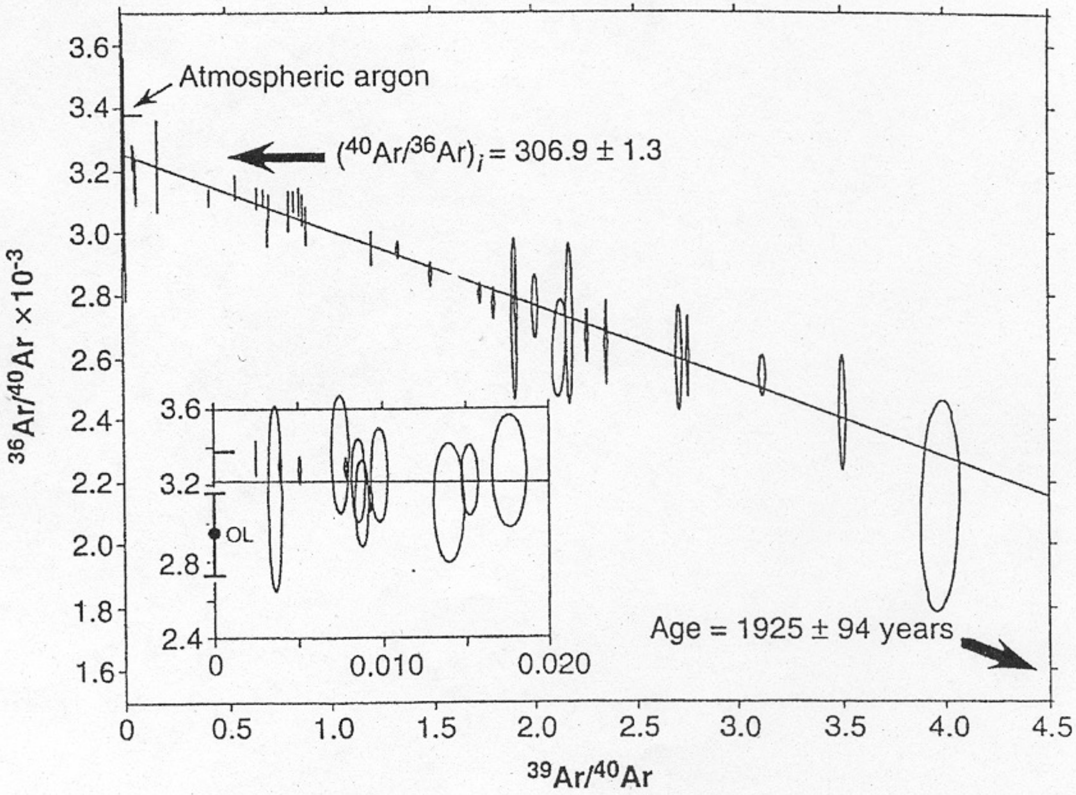

# Inherited argon in young tephra

*Chen, Smith, Evenson, York, Lajoie (1996) Science, v. 274*

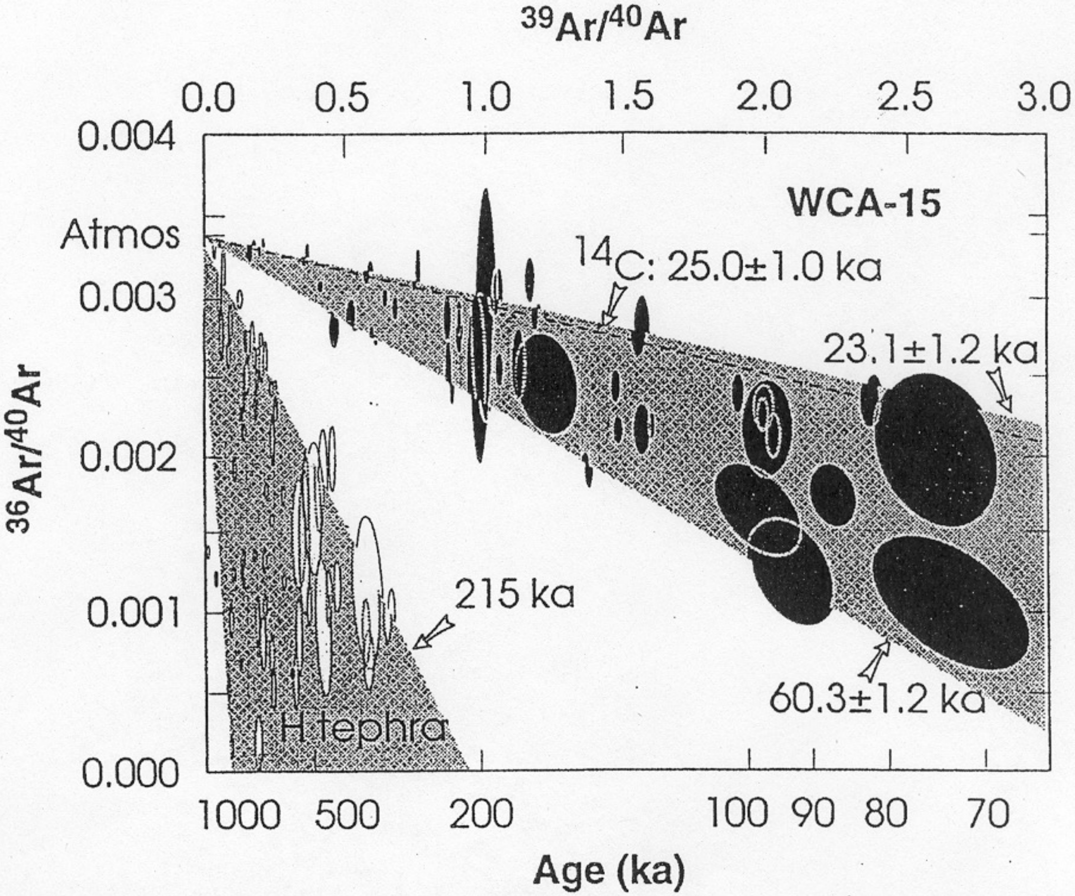


**Fig. 1.** $^{36}Ar/^{40}Ar$ versus $^{39}Ar/^{40}Ar$ correlation diagram for sanidine crystals from ash layer WCA-15 (filled ellipses), and for comparison, earlier analytical results (*16*) from the differentiated Hüttenberg tephra (H tephra) of the East Eifel volcanic field, Germany (open ellipses). All ellipses show 1$\sigma$ analytical errors. Shaded areas are "sphenochrons," bounded by isochrons passing through the $^{36}Ar/^{40}Ar$ ratio of modern atmosphere (=1/295.5). The bounding isochrons for WCA-15 are determined by statistical analysis of the argon data (*10*), with the inferred, corrected $^{14}C$ age of the tephra (*7*) shown as a dashed line for comparison. The upper bound for the H tephra is defined by a 215-ka isochron obtained from anorthoclase crystals from the most mafic lapilli (*16*). See text for further discussion. Note that one small filled ellipse from the WCA-15 ash is within the H tephra region. All data have been normalized to a *J* value of $1.076 \times 10^{-4}$, and the corresponding age scale plotted at the bottom. The integrated age for all WCA-15 data is 38.8 ± 1.1 ka, and is equivalent to the age that would be obtained from a bulk analysis of all the analyzed crystals.

# Rank-order diagrams 'CalTech plots'

- *Used commonly to compare among data sets*

Integrating $^{40}Ar/^{39}Ar$, U-Pb, and astronomical clocks in the Cretaceous Niobrara Formation, Western Interior Basin, USA

Bradley B. Sageman[1†], Brad S. Singer[2], Stephen R. Meyers[2], Sarah E. Siewert[2,3], Ireneusz Walaszczyk[4], Daniel J. Condon[5], Brian R. Jicha[2], John D. Obradovich[6§], and David A. Sawyer[6]

*GSA Bulletin (2014)*

- *Laser fusion data from sandine crystals in Cretaceous bentonites (altered ash beds)*
- *Dates from 10 bentonites, here arranged vertically in stratigraphic order, with corresponding biozones*

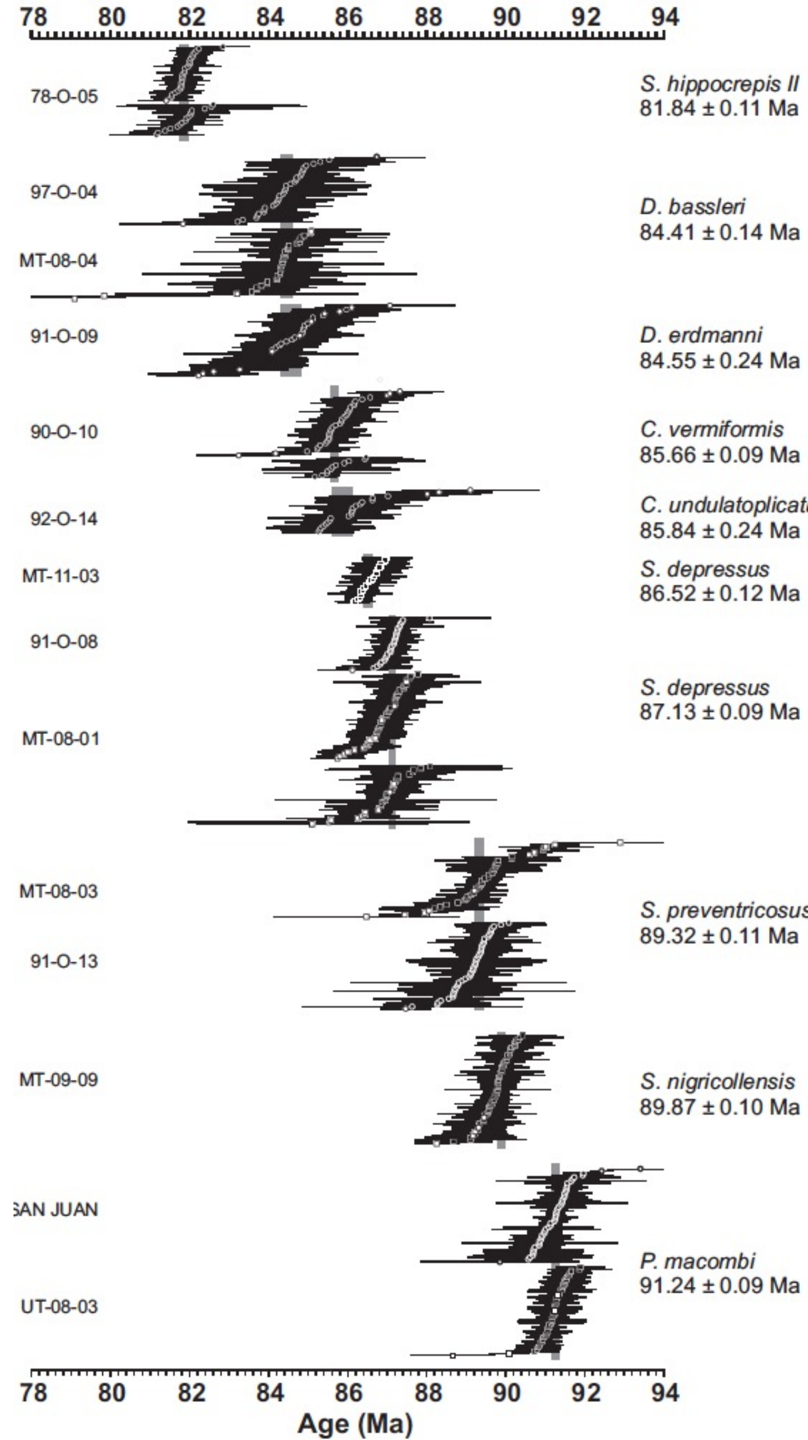

**Probability density diagrams**

- Means of graphically representing results in lieu of conventional box histograms
  - advantage: incorporates and displays variable uncertainties associated with a suite of ages
  - useful for evaluating multiple ages & uncertainties from sub-samples
    - laser total fusions
    - replicate plateau or isochron ages
- Cumulative probability curve
  - sum of all Gaussian probability distributions of individual analyses, based on estimated analytical uncertainties.
  - justified because analytical uncertainties are normally distributed
- Procedure:
  - choose appropriate minimum-maximum age range
  - divide range into intervals, or bins
  - for each age determination with uncertainty ($\sigma$), Gaussian probability (P) is calculated for each bin:

$$P = [1/(2\pi\sigma)^{½}]e^{\Delta^2/2\sigma^2}$$

  - $\Delta$ = difference between bin age and age of the analysis.
  - curve is running tally of cumulative probability for each bin

*Ton That, Singer, Paterne (2001)*
*single sandine crystals from C-13 marine ash bed*

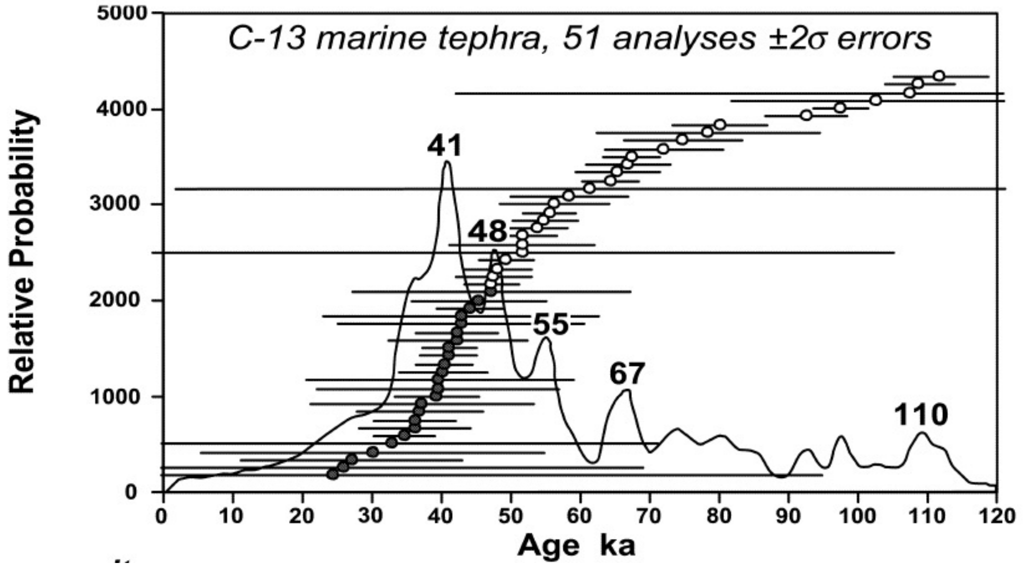


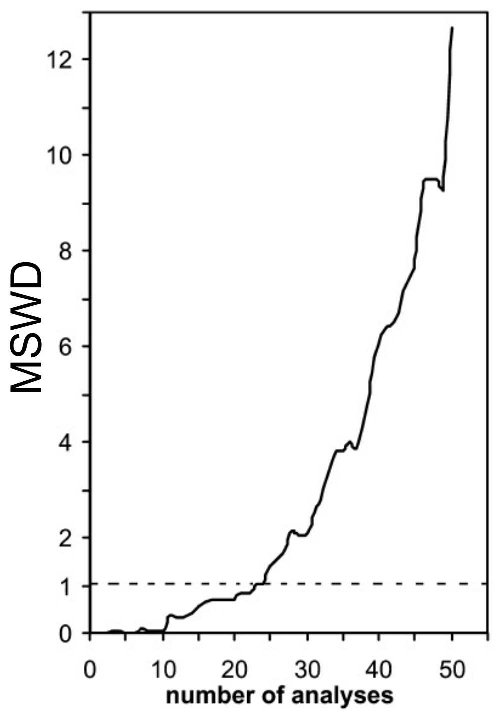

EPSL

Earth and Planetary Science Letters 184 (2001) 645–658

www.elsevier.com/locate/epsl

# $^{40}Ar/^{39}Ar$ dating of latest Pleistocene (41 ka) marine tephra in the Mediterranean Sea: implications for global climate records

Thao Ton-That [a], Brad Singer [b,*], Martine Paterne [c]

[a] Earth Science Institute, University of Geneva, 13 rue des Maraichers, Geneva 1211, Switzerland

[b] Department of Geology and Geophysics, University of Wisconsin-Madison, 1215 West Dayton Street, Madison, WI 53706, USA

[c] Laboratoire des Sciences du Climat et de l'Environnement, Unité mixte CNRS-CEA, Gif sur Yvette 91198, France

Received 10 July 2000; received in revised form 14 November 2000; accepted 17 November 2000



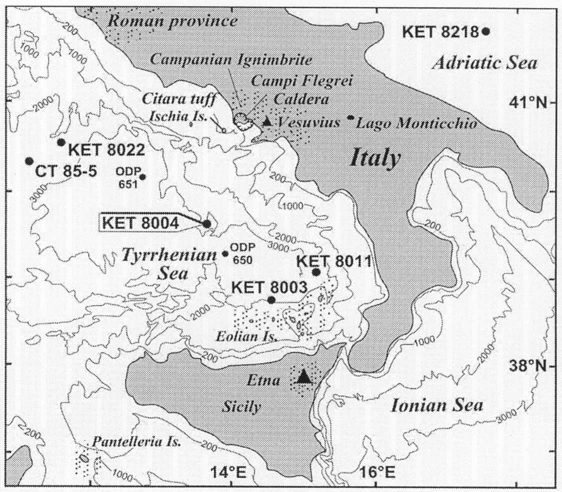


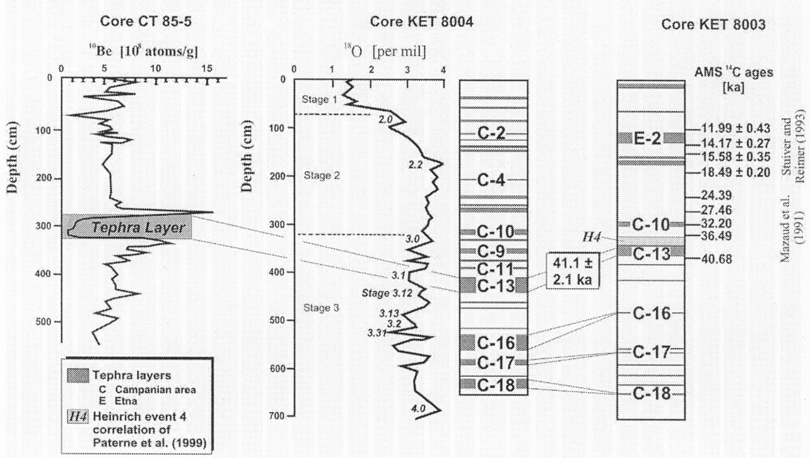




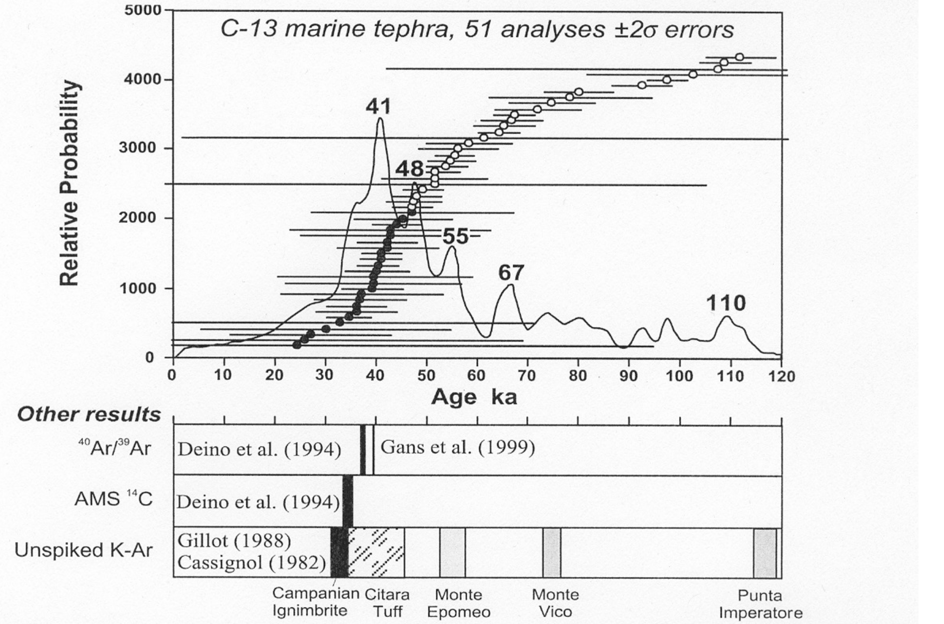


Fig. 3. Probability density plot (ideogram) of apparent ages from tephra layer C-13. Filled symbols denote 24 analyses included in the inverse isochron calculation of Fig. 5. Results from other radioisotopic studies on the Campanian Ignimbrite (black), Citara Tuff (hatched), Monte Epomeo, Monte Vico and Punta Imperatore are discussed in the text.

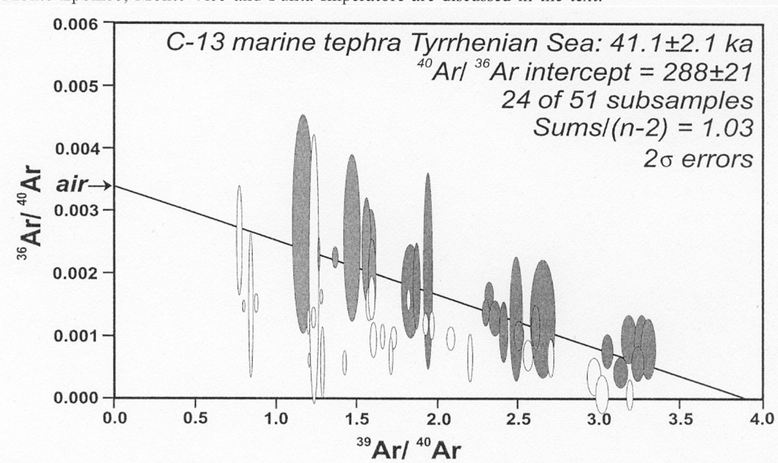


Fig. 5. Inverse isochron diagram of $^{40}Ar/^{39}Ar$ laser heating analyses of sanidine in the C-13 tephra layer. The 24 filled ellipses are analyses included in the regression calculation (see Fig. 4), open ellipses were omitted from calculation.

Available online at www.sciencedirect.com

SCIENCE DIRECT®

Geochimica et Cosmochimica Acta 70 (2006) 426–445

Geochimica

www.elsevier.com/locate/gca

# Reassessing the uranium decay constants for geochronology using ID-TIMS U–Pb data

Blair Schoene [a,*], James L. Crowley [a], Daniel J. Condon [a], Mark D. Schmitz [b], Samuel A. Bowring [a]

**Abstract**

As the internal precision of radiometric dates approaches the 0.1% level, systematic biases between different methods have become apparent. Many workers have suggested that calibrating other decay constants against the U–Pb system is a viable solution to this problem. We test this assertion empirically and quantitatively by analyzing U–Pb systematics of zircon and xenotime on the single- to sub-grain scale by high-precision ID-TIMS geochronology on 11 rock samples ranging from 0.1 to 3.3 Ga. Large statistically equivalent datasets give $^{207}Pb/^{206}Pb$ dates that are systematically older than $^{206}Pb/^{238}U$ dates by ~0.15% in Precambrian samples to as much as ~3.3% in Mesozoic samples, suggesting inaccuracies in the mean values of one or both of the U decay constants. These data are used to calculate a ratio of the U decay constants that is lower than the accepted ratio by 0.09% and is a factor of 5 more precise. Four of the samples are used to augment existing data from which the U–Pb and $^{40}Ar/^{39}Ar$ systems can be compared. The new data support most previous observations that U–Pb and $^{207}Pb/^{206}Pb$ dates are older than $^{40}Ar/^{39}Ar$ by ⩽1%, though scatter in the amount of offset in samples as a function of age suggests that the bias is not entirely systematic, and may incorporate interlaboratory biases and/or geologic complexities. Studies that calibrate other decay schemes against U–Pb should include an assessment of inaccuracies in the U decay constants in addition to other systematic biases and non-systematic geologic uncertainty.

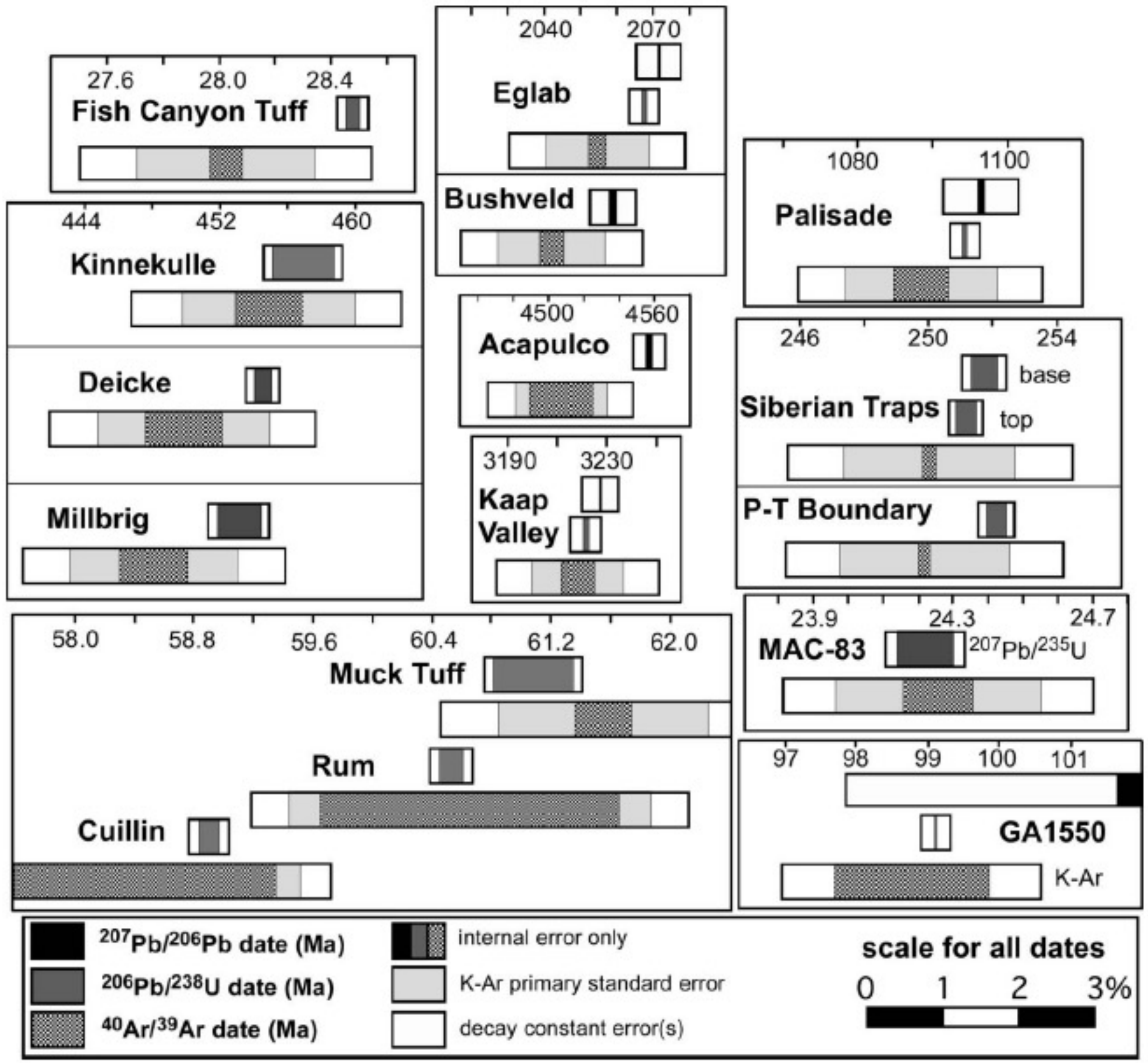


Fig. 4. Summary diagram for U–Pb and $^{40}Ar/^{39}Ar$ dates (in Ma). $^{40}Ar/^{39}Ar$ data are normalized to Fish Canyon sanidine = 28.02 Ma and the primar standard GA1550 $Ar^{*}/K$ values of Renne et al. (1998b). Tracer calibration errors for data from this study are negligible at the shown scale and those fro other studies are not reported. References are given in Table 2. Errors are at the 95% confidence level.

# Synchronizing Rock Clocks of Earth History

K. F. Kuiper,[1,2] A. Deino,[3] F. J. Hilgen,[1] W. Krijgsman,[1] P. R. Renne,[3,4] J. R. Wijbrans[2]

Calibration of the geological time scale is achieved by independent radioisotopic and astronomical dating, but these techniques yield discrepancies of ~1.0% or more, limiting our ability to reconstruct Earth history. To overcome this fundamental setback, we compared astronomical and $^{40}Ar/^{39}Ar$ ages of tephras in marine deposits in Morocco to calibrate the age of Fish Canyon sanidine, the most widely used standard in $^{40}Ar/^{39}Ar$ geochronology. This calibration results in a more precise older age of 28.201 ± 0.046 million years ago (Ma) and reduces the $^{40}Ar/^{39}Ar$ method's absolute uncertainty from ~2.5 to 0.25%. In addition, this calibration provides tight constraints for the astronomical tuning of pre-Neogene successions, resulting in a mutually consistent age of ~65.95 Ma for the Cretaceous/Tertiary boundary.

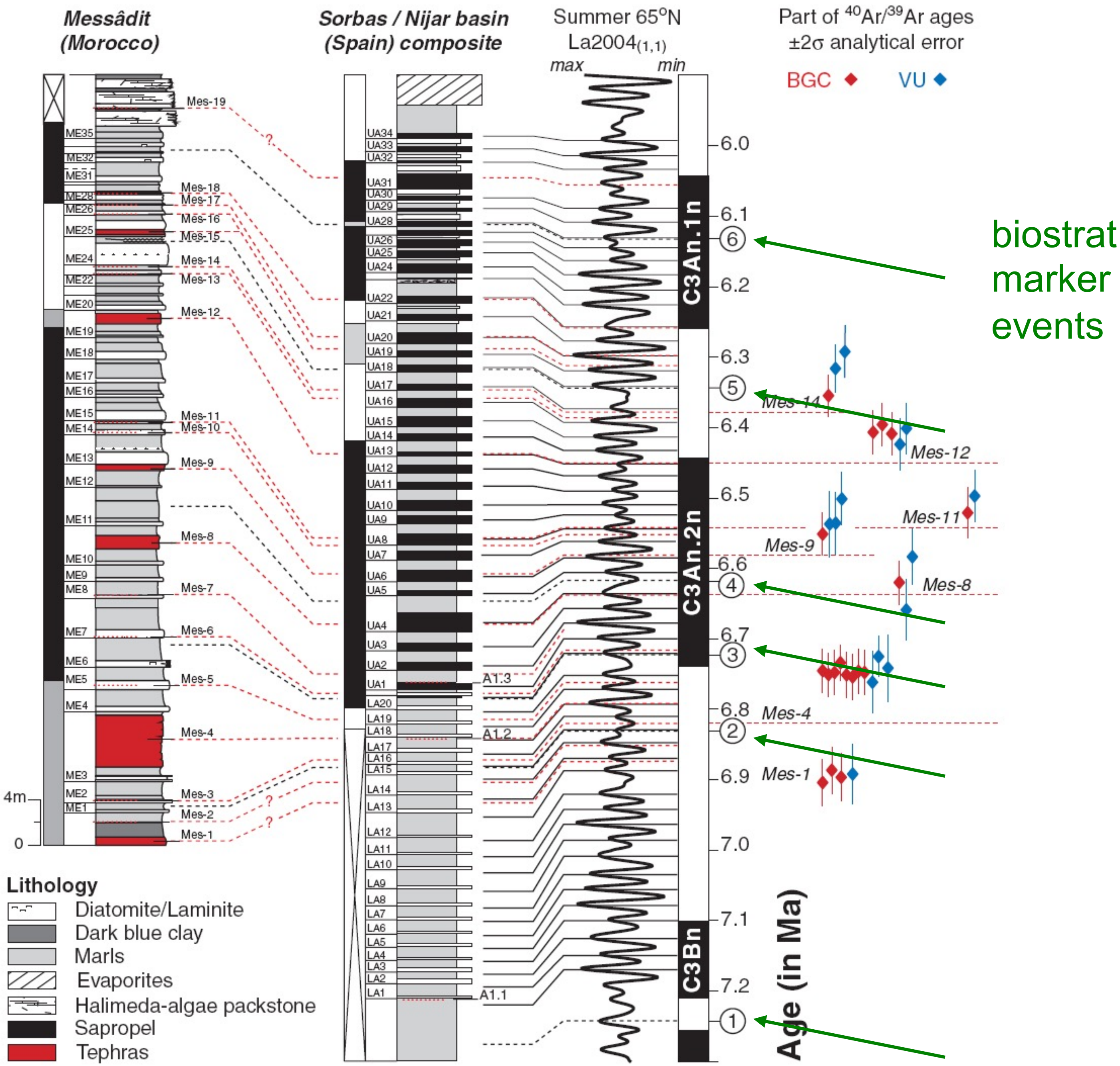


**Fig. 1.** Astronomical calibration of Messinian Messâdit section in the Melilla-Nador Basin and $^{40}Ar/^{39}Ar$ ages of intercalated tephra. The cycles are tuned to the La2004$_{(1,1)}$ solution (*35*). The main biostratigraphic marker events registered within the studied sections and used for high-resolution correlations are (1) *Globorotalia miotumida* group first regular occurrence (FRO), (2) *G. nicolae* first common occurrence (FCO), (3) *G. nicolae* last occurrence (LO), (4) *G. obesa* FCO, (5) *Neogloboquadrina acostaensis* sinistral/dextral coiling change, and (6) *N. acostaensis* first sinistral influx (*11*, *12*, *43*). The phase relation of the sedimentary cycles to orbital parameters is determined using the exact position of bioevents and characteristic planktonic foraminiferal faunal changes associated with the sedimentary cyclicity in the pre-evaporite Messinian Sorbas basin (*43*). Homogeneous marls in the Moroccan sections correspond to sapropels in Sorbas and other Mediterranean sections (*11*). Astronomical ages for the tephras are derived by linear interpolation between two astronomically tuned points (that is, three-quarters of the height from the base of the homogeneous interval in each cycle is correlated to the insolation maximum). Weighted mean $^{40}Ar/^{39}Ar$ ages of tephra intercalated in the Messâdit section and analyzed in BGC and VU are shown, calculated relative to an age of 28.02 Ma for FCs (*4*) (table S1). The 2σ error bars include only analytical uncertainties of samples and standards.

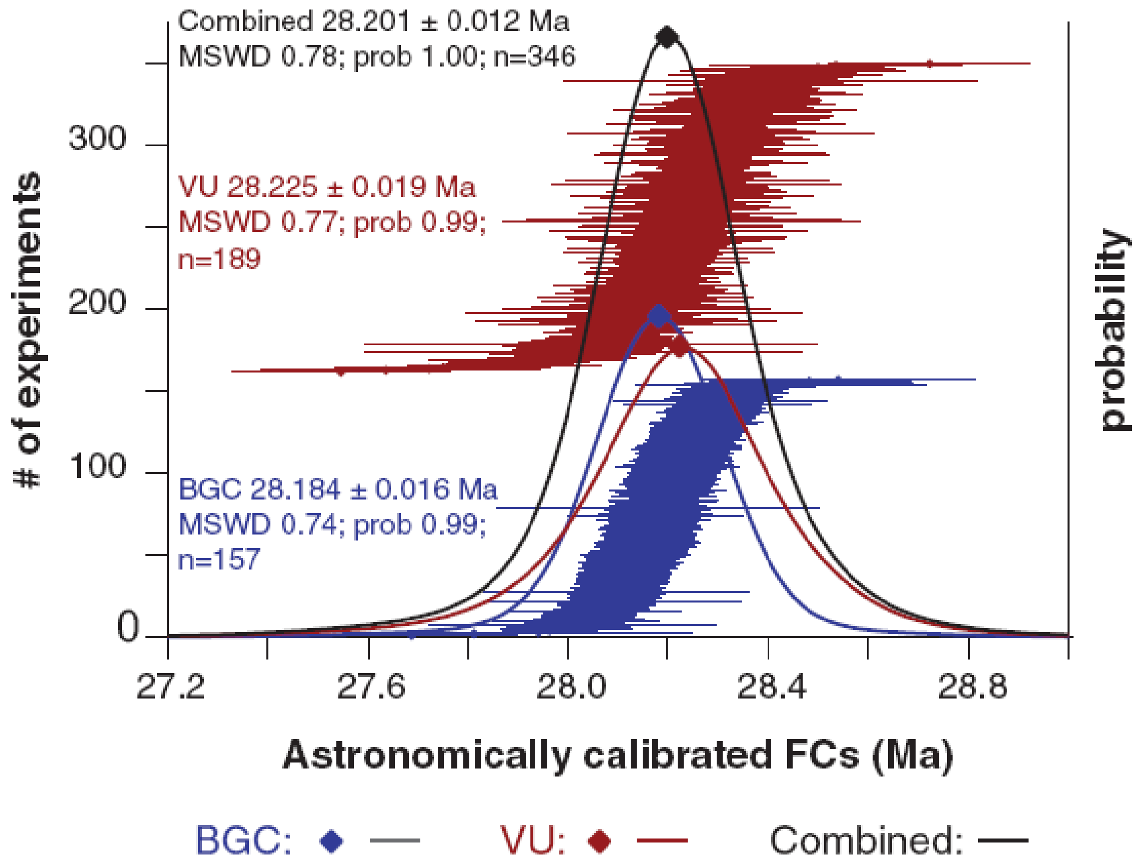


**Fig. 2.** Astronomically calibrated FCs age. The $^{40}Ar/^{39}Ar$ ages of the ash layers are converted to an astronomically calibrated age for FCs by using the Melilla sanidines as astronomically dated standards and the FCs as the unknown. Instead of doing this exercise for each tephra horizon separately, we included all reliably (both isotopic and astronomical) dated tephra to prevent an a priori bias to one of the astronomically dated tephra. However, the calibrated age is an inverse-variance weighted mean age; thus, tephra mes4, with the highest number of replicate analyses and the most precise data, dominates the final outcome. We include only the single-crystal fusion data (displayed here with 1$\sigma$ analytical error), and ages with $P > 0.1$. Incremental heating experiments on selected sanidine fractions confirm the thermally undisturbed nature of the samples (*14*). We calculate an astronomically calibrated FCs age for each experiment propagating only analytical uncertainties. The weighted mean FCs age and standard analytical error for BGC and VU data are displayed separately and as a combined-age probability diagram. The 28.201 ± 0.012 Ma age for FCs is converted to an intercalibration factor of $R^{FCs}_{astro}$ of 4.3644 ± 0.0018 for a $T_{astro}$ at 6.500 Ma. This translates to 28.201 ± 0.046 Ma, including decay-constant uncertainties and the uncertainty in the astronomical ages of ±10 ky.

ELSEVIER
Available online at www.sciencedirect.com
ScienceDirect
Geochimica et Cosmochimica Acta 74 (2010) 5349–5367
Geochimica et Cosmochimica Acta
www.elsevier.com/locate/gca

# Joint determination of $^{40}K$ decay constants and $^{40}Ar^*/^{40}K$ for the Fish Canyon sanidine standard, and improved accuracy for $^{40}Ar/^{39}Ar$ geochronology

Paul R. Renne[a,b,*], Roland Mundil[a], Greg Balco[a,b], Kyoungwon Min[c], Kenneth R. Ludwig[a]

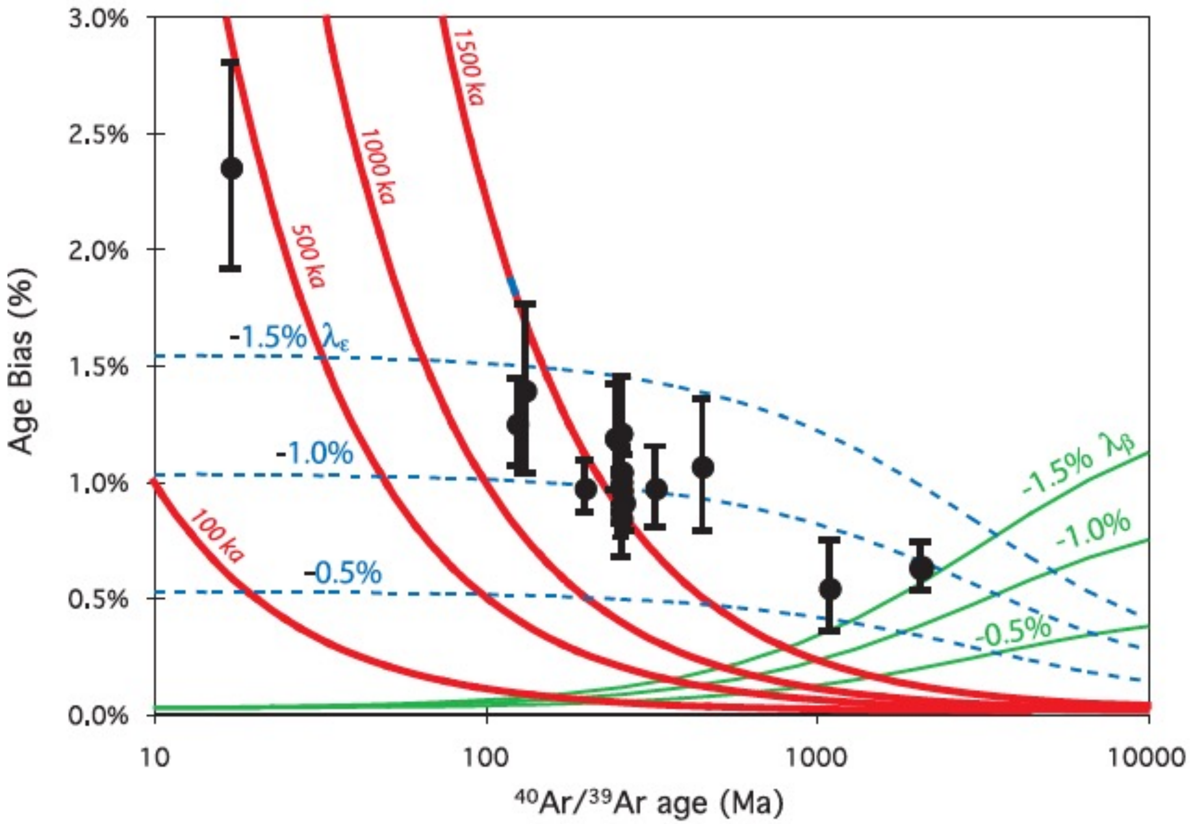


- *1% bias between $^{40}Ar/^{39}Ar$ ages calibrated using FCs at 28.02 Ma and 16 U-Pb zircon ages from quickly cooled rocks*
- *'Optimization' algorithm used to determine age for FCs that eliminates this bias*
- *FCs = 28.294 Ma*

*Schmitz and Kuiper (2012) modified from Renne et al. (2010)*

# U-Pb and $^{40}Ar/^{39}Ar$ ages of Fish Canyon Tuff re-examined in 2013

## Tracking the evolution of large-volume silicic magma reservoirs from assembly to supereruption

Jörn-Frederik Wotzlaw[1]*, Urs Schaltegger[1], Daniel A. Frick[2], Michael A. Dungan[1,3], Axel Gerdes[4,5], and Detlef Günther[2]

ABSTRACT

The most voluminous silicic volcanic eruptions in the geological past were associated with caldera collapses above giant silicic magma reservoirs. The thermal evolution of these sub-caldera magma reservoirs controls the volume of eruptible magma and eruptive style. Here we combine high-precision zircon U-Pb geochronology, trace element analyses of the same mineral grains, and mass balance modeling of zircon trace element compositions allowing us to track the thermal and chemical evolution of the Oligocene Fish Canyon Tuff magma reservoir (Colorado, United States) as a function of absolute time. Systematic compositional variations in U-Pb dated zircons record ~440 k.y. of magma evolution. An early phase of volumetric growth was followed by a period of cooling and crystallization, during which the Fish Canyon magma approached complete solidification. Subsequent remelting, due to underplated andesitic recharge magmas, began 219 ± 45 k.y. prior to eruption, and led to the generation of ~5000 km³ of eruptible crystal-rich (~45 vol%) dacite. Age-equivalent, but compositionally different, zircons in an andesite enclave from late-erupted Fish Canyon Tuff tie the growth and thermal evolution of the upper-crustal reservoir to a lower-crustal magma processing zone. Our results demonstrate that the combination of high-precision dating and trace element analyses of accessory zircons can reveal invaluable information about the chemical and thermal histories of silicic magmatic systems and provides critical input parameters for fluid dynamic modeling.

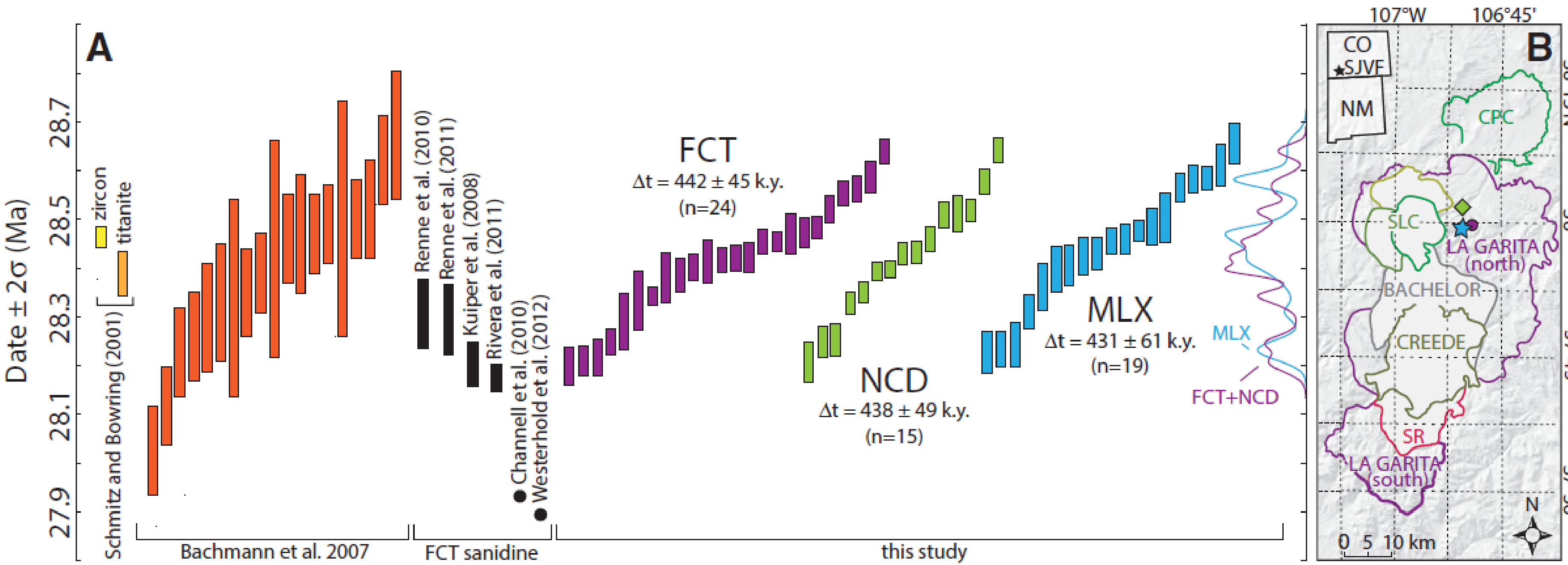


Figure 1. Geochronology of the Fish Canyon (Colorado, United States) magmatic system. A: Comparison of previously published zircon and titanite U-Pb and sanidine $^{40}Ar/^{39}Ar$ dates with zircon U-Pb dates obtained in this study. All U-Pb dates are $^{206}Pb/^{238}U$ dates corrected for initial $^{238}U$-$^{230}Th$ disequilibrium using $Th/U_{melt}$ of 2.2 (Schmitz and Bowring, 2001). Δt denotes age difference between oldest and youngest zircon date of each sample. Probability density functions show distribution of $^{206}Pb/^{238}U$ dates. FCT—Fish Canyon Tuff; NCD—Nutras Creek Dacite; MLX—andesite enclave. B: Caldera map of the Central San Juan caldera cluster showing locations of samples analyzed in this study; inset map (top left) shows location of San Juan volcanic field (SJVF) within the state of Colorado. CPC—Cochetopa Park caldera; SLC—San Luis complex; SR—South River caldera.

# An EARTHTIME-Calibrated $^{40}Ar/^{39}Ar$ Laboratory

Alder Creek Rhyolite sanidine (ACs-2) standard

Jicha, SInger, Sobol (2016) Chemical Geology

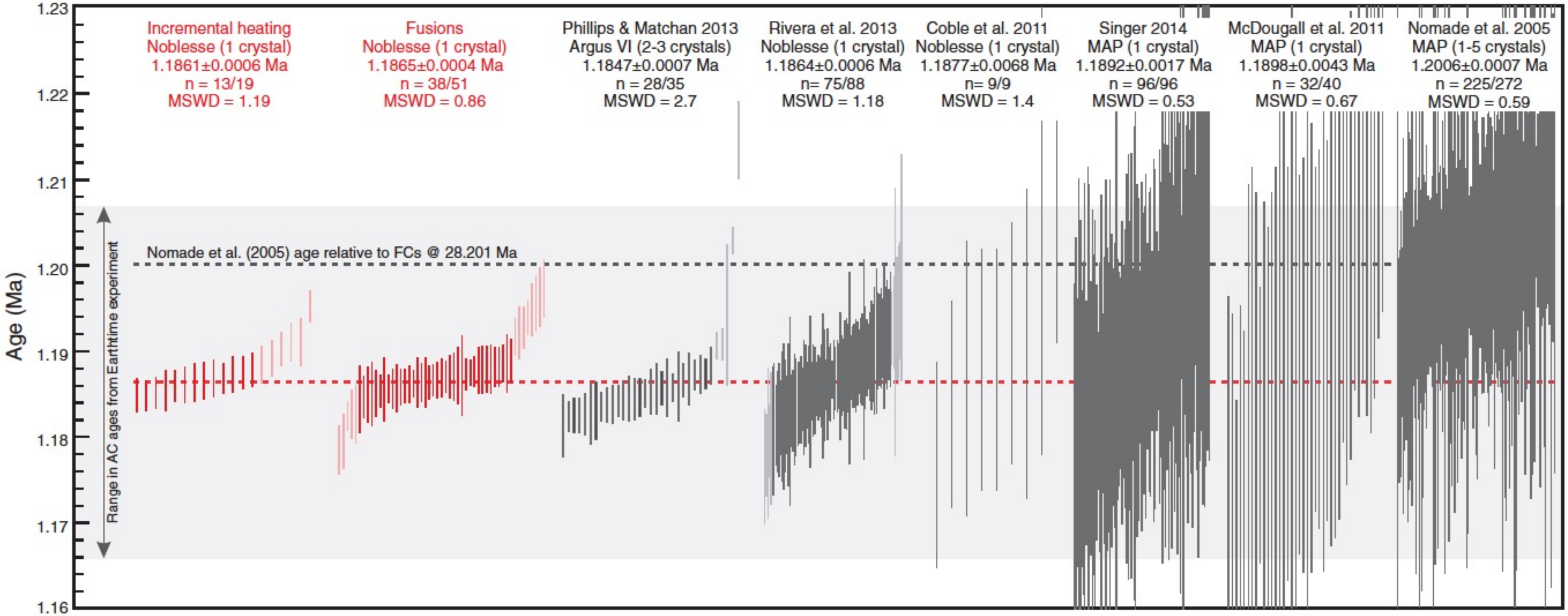


**Fig. 4.** Comparison of $^{40}Ar/^{39}Ar$ ages determined for Alder Creek rhyolite sanidine sample ACs-2 since 2005. $^{40}Ar/^{39}Ar$ ages are shown with $\pm 2\sigma$ analytical uncertainties only. Some of the published ages have been recalculated so that all the data in this figure are relative to 28.201 Ma for the Fish Canyon sanidine. The commonly used age from Nomade et al. (2005) is shown as a dotted line. Gray band indicates range in ages generated during the EARTHTIME laboratory intercalibration experiment (Heizler and EARTHTIME working group, 2008). Recent experiments including all the data collected using multi-collector mass spectrometers (Phillips and Matchan, 2013; Rivera et al., 2013) give ages that are significantly younger than the Nomade et al. (2005) age. Our preferred age (red dotted line) for AC-2 based on a weighted mean of the Rivera et al. (2013) dates and our plateau ages and total fusion dates is $1.1864 \pm 0.0003/0.0012$ Ma (95% confidence analytical/full external).
Data sources: Phillips and Matchan (2013); Rivera et al. (2013); Coble et al. (2011); Singer (2014); McDougall et al. (2011); Nomade et al. (2005).

# An EARTHTIME-Calibrated $^{40}Ar/^{39}Ar$ Laboratory

Fish Canyon Tuff sanidine (FCs) standard
Jicha, SInger, Sobol (2016) Chemical Geology

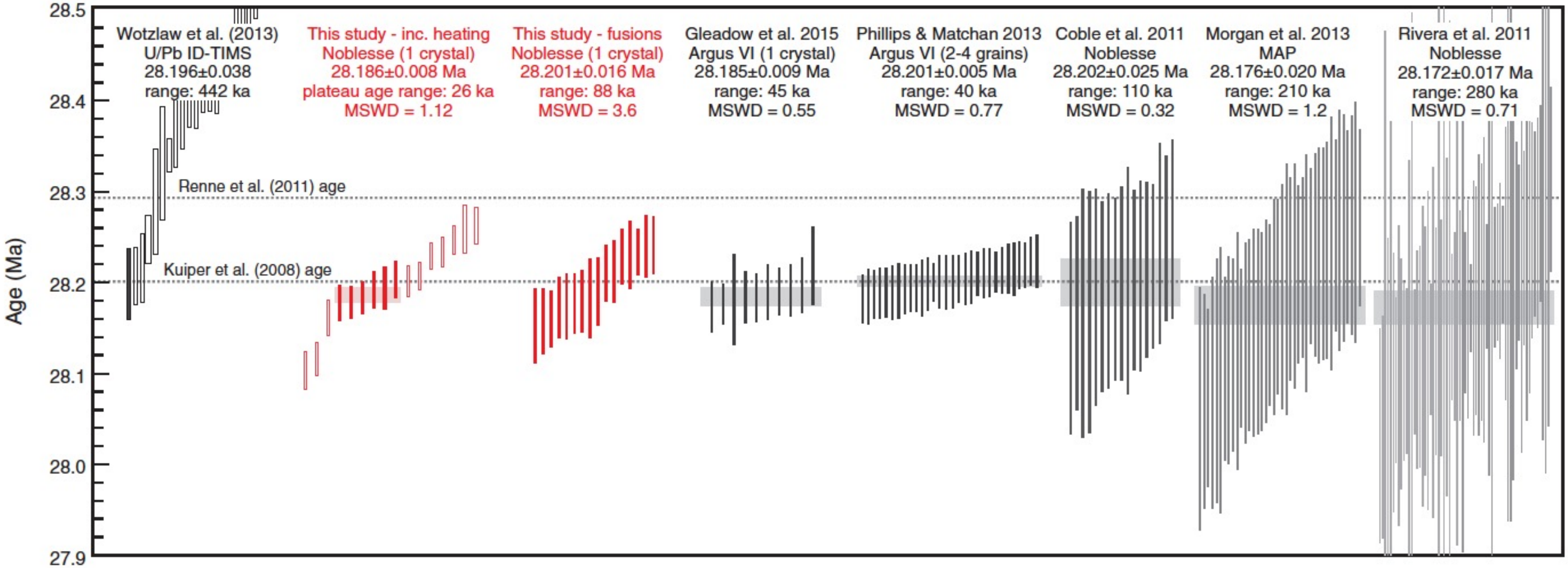


**Fig. 7.** Comparison of $^{40}Ar/^{39}Ar$ ages determined for Fish Canyon sanidine sample FC-2. All $^{40}Ar/^{39}Ar$ ages are shown with analytical uncertainties only and are relative to 28.201 Ma for the Fish Canyon sanidine (Kuiper et al., 2008). Note that all total fusion data were performed on single crystals except for that of Phillips and Matchan (2013), which fused 2–4 crystals per analysis. Our single crystal total fusion experiments gave a range in dates spanning ~88 ka and thus have a MSWD of 3.6. Overall the range in dates is similar to those of the previous studies. Only 6 of the 16 single crystal incremental heating experiments gave statistically acceptable plateaus (filled red boxes). A weighted mean age of these 6 plateaus is 28.186 ± 0.008 Ma. The total fusion ages for the crystals which did not yield plateaus are shown as open boxes. CA-IDTIMS U–Pb zircon dates are from Wotzlaw et al. (2013); the youngest zircon (solid black bar) is 28.196 ± 0.038 Ma. We recognize that there are other published U–Pb zircon datasets for the Fish Canyon Tuff. However, the purpose of the figure is to highlight the age complexity within the FCT not select an absolute age for the FCT.
Data sources: Wotzlaw et al. (2013); Gleadow et al. (2015); Phillips and Matchan (2013); Coble et al. (2013); Morgan et al. (2013); Rivera et al. (2011).